

1 **CRK2-mediated control of ROS production by phosphorylation of the** 2 **RBOHD C-terminus in Arabidopsis**

3
4 Sachie Kimura¹, Kerri Hunter¹, Lauri Vaahtera², Cuong Tran^{1#}, Aleksia Vaattovaara¹, Anne Rokka³, Sara
5 Christina Stolze⁴, Anne Harzen⁴, Lena Meißner^{1§}, Maya Wilkens^{1§}, Thorsten Hamann², Masatsugu Toyota^{5,6},
6 Hirofumi Nakagami⁴, Michael Wrzaczek^{1*}

7
8 ¹Organismal and Evolutionary Biology Research Programme, Viikki Plant Science Centre, Faculty of
9 Biological and Environmental Sciences, University of Helsinki, Helsinki, FI-00014, Finland.

10 ²Department of Biology, Norwegian University of Science and Technology, 7491 Trondheim, Norway.

11 ³Turku Centre for Biotechnology, University of Turku and Åbo Akademi, FI-20520, Finland.

12 ⁴Protein Mass Spectrometry Group, Max-Planck Institute for Plant Breeding Research, Carl-von-Linné-Weg
13 10, D-50829 Cologne, Germany.

14 ⁵Department of Biochemistry and Molecular Biology, Saitama University, Saitama 338-8570, Japan.

15 ⁶Department of Botany, University of Wisconsin, Madison, WI, 53593, USA.

16 #Present address: Department of Biology, Lund University, Sölvegatan 35, 223 62 Lund, Sweden.

17 §Present address: Technische Universität Braunschweig, Germany.

18
19 * To whom correspondence should be addressed:

20 Michael Wrzaczek

21 Organismal and Evolutionary Biology Research Programme

22 Viikki Plant Science Centre, VIPS

23 Faculty of Biological and Environmental Sciences

24 Viikinkaari 1, PO Box 65

25 FIN-00014 Helsinki University

26 Finland

27 Email: michael.wrzaczek@helsinki.fi

28 Phone: +358 2941 57 773

29
30 ORCID IDs: 0000-0001-5736-2123 (SK), 0000-0002-2285-6999 (KH), 0000-0003-4733-4430 (LV), 0000-
31 0002-7670-2215 (CT), 0000-0003-3452-0947 (AV), 0000-0003-1482-9154 (AR), 0000-0002-1421-9703
32 (SCR), 0000-0002-8605-6026 (LM), 0000-0003-4631-6177 (Mwi), 0000-0001-8460-5151 (TH), 0000-
33 0002-9544-0978 (MT), 0000-0003-2569-7062 (HN), 0000-0002-5946-9060 (MWR)

34 **Abstract**

35 **Reactive oxygen species (ROS) are important messengers in eukaryotic organisms and their**
36 **production is tightly controlled. Active extracellular ROS production by NADPH oxidases in plants is**
37 **triggered by receptor-like protein kinase (RLK)-dependent signaling networks. Here we show that the**
38 **cysteine-rich RLK CRK2 exists in a preformed complex with the NADPH oxidase RBOHD at the**
39 **plasma membrane in Arabidopsis. Functional CRK2 is required for the full pathogen-induced ROS**
40 **burst and consequently the *crk2* mutant is impaired in defense against the bacterial pathogen**
41 ***Pseudomonas syringae* pv. tomato DC3000. We identified phosphorylation sites in the C-terminal**
42 **region of RBOHD and mutations of these phosphorylation sites alter ROS production in response to**
43 **biotic stimuli. Our work demonstrates that CRK2 regulates elicitor-triggered ROS production. We**
44 **propose that regulation of NADPH oxidase activity by phosphorylation of the C-terminal region is an**
45 **ancient mechanism and phospho-sites are conserved throughout the plant lineage and between**
46 **animals and plants.**

47 **Introduction**

48 Plants are continuously confronted with stimuli from the surrounding environment, including abiotic cues
49 and invading pathogens. Plant cells also perceive a plethora of signals from neighbouring cells and distant
50 tissues. Numerous plasma membrane proteins are involved in the meticulous monitoring and transduction of
51 signals for inter- and intracellular communication. A common early feature of many cellular responses to
52 various environmental changes involves the production of reactive oxygen species (ROS)^{1,2}. While ROS are
53 an inevitable by-product of aerobic metabolism² and their unrestricted accumulation can have deleterious
54 consequences², ROS are also ubiquitous signaling molecules in plants and animals alike^{2,3}. Eukaryotic cells
55 produce ROS in several subcellular compartments as well as the extracellular space, in plants referred to as
56 apoplast^{1,2}. A major component in the production of extracellular ROS is the evolutionarily conserved
57 NADPH oxidase (NOX) family^{1,4}. NOX-dependent ROS production is involved in regulation of immune
58 functions, cell growth and apoptosis in animals and plants^{2,5}.

59 Plant NOXs, referred to as respiratory burst oxidase homologs (RBOHs), have been identified as homologs
60 of phagocyte gp91^{phox}/NOX2, which contains six transmembrane helices and a C-terminal NADPH- and
61 FAD-binding cytoplasmic region⁶. Unlike gp91^{phox}/NOX2, RBOHs contains an additional N-terminal region
62 with Ca²⁺-binding EF-hands, similar to non-phagocytic NOXs, such as NOX5³. RBOH activity is strictly
63 controlled to avoid damaging consequences of unrestricted ROS production³. *Arabidopsis thaliana*
64 (*Arabidopsis*) RBOHD is the best-characterized RBOH and is involved in biotic and abiotic stress
65 responses⁶⁻⁸. The N-terminal region of RBOHD is phosphorylated by a variety of protein kinases, including
66 receptor-like cytoplasmic kinases (RLCKs)⁹⁻¹⁶, for example BOTRYTIS-INDUCED KINASE 1 (BIK1)^{11,12}.
67 While previous research has suggested a predominant role of phosphorylation of the N-terminal region for
68 regulation of RBOH, phosphorylation of the C-terminal region is important for the regulation of human
69 gp91^{phox}/NOX2 and NOX5^{17,18}. NADPH- and FAD-binding sites in C-terminus are highly conserved in
70 NOXs and RBOHs, but it is unclear whether the C-terminus of plant RBOHs could also be a target for
71 regulation of the ROS producing activity.

72 Apoplastic RBOH-dependent ROS production is a common response to the activation of receptor-like
73 protein kinase (RLK)¹⁹ signaling, in particular following perception of microbe-associated molecular patterns
74 (MAMPs) or damage-associated molecular patterns (DAMPs)^{1,20}. However, the role of the so-called ROS
75 burst and its integration into RLK-triggered signaling networks are as yet unclear¹. A large group of RLKs in
76 plants is formed by the cysteine-rich RLKs (CRKs)²¹. The extracellular region of CRKs harbors two copies
77 of the domain of unknown function 26 (DUF26) but the molecular function of the CRK ectodomain remains
78 unknown²¹. CRKs have been linked to ROS signaling²²⁻²⁵ and cell death^{24,26} and are important signaling
79 elements in plant development, biotic and abiotic stress responses²²⁻³¹.

80 Here we characterize the role of CRK2 in immune signaling in response to MAMP-perception. CRK2 exists
81 in a pre-formed complex with RBOHD at the plasma membrane. CRK2 controls the activity of RBOHD and

82 functional CRK2 is required for full MAMP-induced ROS production. Importantly, we show that CRK2
83 phosphorylates the C-terminal region of RBOHD and modulates the ROS-production activity of RBOHD *in*
84 *vivo*. Our results lead us to propose a novel mechanism for the regulation of RBOHD activity through
85 phosphorylation of the C-terminal region and highlight a critical role for CRK2 in the precise control of the
86 ROS burst in response to biotic stress.

87 **Results**

88 **CRK2 kinase activity is important for plant development**

89 CRK2 has been previously implicated in stress responses and development in *Arabidopsis*²⁵. CRK2 is a
90 typical CRK with N-terminal signal peptide, extracellular region containing two DUF26 domains,
91 transmembrane region and intracellular protein kinase domain (Fig. 1a). The *crk2* mutant was smaller than
92 wild type (Col-0) plants (Fig. 1b), and displayed significantly reduced fresh (Fig. 1c) and dry weight (Fig.
93 S1a). Over-accumulation of the plant hormone salicylic acid (SA) often causes a reduction of plant size, but
94 SA levels were not significantly different between *crk2* and wild type plants (Fig. S1b). Expression of YFP-
95 tagged CRK2 under the control of the CRK2 promoter (*CRK2pro::CRK2-YFP*) in the *crk2* background
96 restored plant growth (Figs. 1b, 1c and S1a). CRK2 is an active protein kinase capable of phosphorylating
97 the generic substrate myelin basic protein (MyBP) *in vitro* (Fig. S1c). To investigate whether the kinase
98 activity of CRK2 was required for restoring the smaller size of the *crk2* back to wild type levels, we
99 generated two different enzymatically inactive (kinase-dead) versions of CRK2 and introduced them into the
100 *crk2* mutant: the ATP-binding lysine (K) at position 353 was substituted with glutamic acid (E; CRK2^{K353E})
101 while the aspartic acid (D) at position 450 in the catalytic domain VIB³² was substituted with asparagine (N;
102 CRK2^{D450N}; Fig. 1a and S1c). Expression of CRK2^{K353E}-YFP or CRK2^{D450N}-YFP under control of the *CRK2*
103 promoter failed to restore the growth defect of *crk2* (Figs. 1b, 1c and S1a). The amino acid substitutions did
104 not alter subcellular localization at plasma membrane as kinase-dead CRK2 variants displayed the same
105 subcellular localization as wild type CRK2-YFP (Figs. 1d and S1d). In summary, our results show that
106 CRK2 is important for proper plant growth and its kinase activity is crucial for this function.

107 **CRK2 is required for MAMP-triggered responses and resistance to *Pseudomonas syringae* pv. tomato 108 DC3000**

109 Previous results suggested that ROS production triggered by flg22, a MAMP derived from bacterial flagella,
110 is reduced in *crk2*²⁵. Therefore, we tested the role of CRK2 in MAMP-induced ROS production in detail.
111 ROS production triggered by flg22 was reduced in *crk2* and reintroduction of CRK2-YFP into the mutant
112 background restored ROS production to the same levels as in Col-0 (Fig. 2a). The flg22-induced ROS
113 production in plants expressing CRK2^{D450N}-YFP was comparable to *crk2* (Fig. 2b). Transcriptional
114 upregulation of flg22 responsive genes (*FRK1* and *NHL10*) showed that MAMP-perception was not impaired
115 in *crk2* (Figs. S2a and S2b). To test whether the reduced response of *crk2* to flg22 was accompanied by
116 altered pathogen susceptibility, we measured growth of the hemibiotrophic bacterial pathogen *Pseudomonas*
117 *syringae* DC3000 pv. tomato (*Pto* DC3000). The *crk2* mutant was significantly more susceptible to the
118 virulent pathogen compared to Col-0 (Fig. 2c). CRK2-YFP but not the kinase-dead CRK2^{D450N}-YFP restored
119 the pathogen susceptibility of *crk2* (Fig. 2c). ROS production induced by chitin (Fig. S2c) and pep1 (Fig.
120 S2d) was also reduced in *crk2* compared to Col-0 suggesting that the reduced MAMP-triggered ROS
121 production in *crk2* is a general response and not specific to flg22.

122 To investigate the role of CRK2 in flg22-triggered responses in more detail, we assessed Ca^{2+} signaling,
123 MAPK activation and callose deposition in *crk2*. Application of flg22 resulted in a rapid increase in cytosolic
124 Ca^{2+} ($[\text{Ca}^{2+}]_{\text{cyto}}$) levels in wild type plants, which express the FRET-based Ca^{2+} -sensor *YCNano65*³³. This
125 response was strongly reduced in the *crk2* mutant background, *YCNano65/crk2* (Figs. 2d and 2e).
126 Interestingly, flg22-dependent MAPK activation (Fig. S2e) and callose deposition (Fig. S2f and g) were
127 more pronounced in *crk2* compared to Col-0. Taken together, CRK2 is an essential component for mounting
128 immune responses against the virulent bacterial pathogen in Arabidopsis, modulating extracellular ROS
129 production, callose deposition, Ca^{2+} influx and MAPK activation.

130 **CRK2 interacts with RBOHD and controls ROS production**

131 RBOHD is the main source of MAMP/DAMP-induced extracellular ROS production^{1,20} and flg22-, pep1 and
132 chitin-induced ROS production was significantly reduced in *crk2* (Figs. 2 and S2). RBOH proteins, including
133 RBOHD, are synergistically activated by protein phosphorylation and Ca^{2+} -binding to EF-hand motifs in the
134 N-terminal region⁹. Given the importance of the kinase activity of CRK2 in MAMP-induced ROS production
135 we investigated whether CRK2 could activate RBOHD. To test this, we used human embryonic kidney 293T
136 (HEK293T) cells, a human cell culture which produces minimal amounts of extracellular ROS due to a lack
137 of expression of endogenous NADPH oxidases¹⁶. HEK293T cells were co-transfected with *3FLAG-RBOHD*
138 and *CRK2-3Myc* or *3Myc-GFP* as control. Subsequently, RBOHD-mediated extracellular ROS production
139 was measured by luminol-amplified chemiluminescence. Despite equal 3FLAG-RBOHD protein levels (Fig.
140 S3a) ROS production in cells co-transfected with *CRK2-3Myc* and *3FLAG-RBOHD* was strongly elevated
141 compared to cells co-transfected with *3FLAG-RBOHD* and *3Myc-GFP* (Fig. 3a). Co-transfection with the
142 inactive variant *CRK2^{D450N}-3Myc* did not enhance ROS production by *3FLAG-RBOHD* compared to co-
143 transfection with *CRK2-3Myc* (Fig. 3a). Transfection of *CRK2-3Myc* in the absence of *3FLAG-RBOHD* did
144 not induce ROS production in HEK293T cells (Fig. 3a). Since RBOHD can also be activated by Ca^{2+} ,
145 HEK293T cells were treated with ionomycin, a Ca^{2+} ionophore that induces a rise in cytosolic Ca^{2+} levels.
146 Ionomycin-induced transient ROS production (Δ_{delta} ROS: $\text{ROS}_{\text{T}=30}$ to $\text{ROS}_{\text{T}=31}$) in *CRK2-3Myc* and *3FLAG-*
147 *RBOHD* co-transfected cells was not different from *3Myc-GFP* and *3FLAG-RBOH* co-transfected cells (Fig.
148 3a). Activation of RBOHD activity by CRK2 was not dependent on Ca^{2+} influx as the elevated basal ROS
149 production activity of RBOHD co-transfected with *CRK2-3Myc* ($\text{ROS}_{\text{T}=0}$ to $\text{ROS}_{\text{T}=30}$ in Fig. 3a) was also
150 observed when using Ca^{2+} -free assay buffer (Figs. S3b and S3c). These results suggest that *CRK2-3Myc*
151 enhanced the basal ROS-producing activity of 3FLAG-RBOHD in HEK293T cells uncoupling it from Ca^{2+}
152 dependence.

153 The Arabidopsis genome encodes 10 *RBOHs*⁹. To test whether CRK2 specifically activates RBOHD, CRK2-
154 3Myc was co-transfected with RBOHF and RBOHC into HEK293T cells. CRK2-3Myc enhanced basal
155 ROS-producing activity of RBOHC and RBOHF in HEK293T cells similarly to RBOHD (Figs. S3d-S3g).
156 However, while the basal ROS production activity ($\text{ROS}_{\text{T}=5}$) of RBOHD and F was elevated approximately

157 10fold, the basal activity of RBOHC was only elevated 3fold suggesting that CRK2 exhibited a preference
158 for RBOHD and F in the heterologous HEK293T cell system.

159 To investigate whether CRK2 and RBOHD interact *in planta*, we performed co-immunoprecipitation (Co-IP)
160 assays using *rbohD* plants expressing *35S::CRK2-YFP* and *35S::FLAG-RBOHD*. CRK2-YFP was
161 immunoprecipitated using an anti-GFP antibody coupled to magnetic beads and co-purified RBOHD was
162 detected using a RBOHD-specific antibody. RBOHD co-purified with CRK2 (Fig. 3b) and treatment of
163 plants with flg22 did not alter the interaction of CRK2 with RBOHD (Fig. 3c). The co-immunoprecipitation
164 result was supported by bimolecular fluorescence complementation (BiFC) assays in *Nicotiana benthamiana*.
165 Leaves transfected with NmVen210::RBOHD - CRK2::CVen210 but not the negative control
166 (NmVen210::RBOHD - GUS::CVen210) exhibited fluorescence at the cell periphery (Fig. S3h) suggesting
167 that CRK2 interacted with RBOHD at the plasma membrane. To analyze this interaction in more detail, we
168 carried out *in vitro* interaction assays between the cytosolic region of CRK2 (Fig. 1a) and the cytosolic N-
169 terminal and C-terminal regions of RBOHD (Fig. 3d). Recombinant RBOHD/N or RBOHD/C tagged with
170 6His and maltose-binding protein (MBP; 6His-MBP-RBOHD/N, 6His-MBP-RBOHD/C) or MBP were
171 incubated with the cytosolic region of CRK2, which contains the kinase domain (CRK2_{cyto}) tagged with
172 6His and glutathione S-transferase (GST; 6His-GST-CRK2_{cyto}) and glutathione sepharose beads. GST pull-
173 down assay showed that 6His-GST-CRK2_{cyto} interacted *in vitro* with 6His-MBP-RBOHD/N but
174 intriguingly also with 6His-MBP-RBOHD/C (Fig. 3e). In summary, our results suggest that CRK2 is capable
175 of direct interaction with RBOHD. CRK2 and RBOHD form a complex which exists independent of flg22
176 perception *in planta*, in contrast to many other RLK-containing complexes which are formed in response to
177 ligand-binding.

178 **CRK2 phosphorylates RBOHD *in vitro***

179 The kinase activity of CRK2 was essential for the full flg22-triggered ROS burst *in planta* as well as for
180 enhancing ROS production by RBOHD in HEK293T cells. Therefore, we tested whether CRK2 could
181 phosphorylate RBOHD *in vitro*. Recombinant 6His-GST-CRK2_{cyto} and 6His-MBP tagged RBOHD
182 cytosolic regions (Figs. 1a and 3d) were produced in *E. coli* and affinity purified. The 6His-GST-CRK2_{cyto}
183 phosphorylated 6His-MBP-RBOHD/N but not MBP (Fig. 4a), similar to the phosphorylation of RBOHD by
184 BIK1, which was used as positive control (Fig. S4). Because of the similar molecular weight of 6His-GST-
185 CRK2_{cyto} (68.5 kDa) and 6His-MBP-RBOHD/C (78.4 kDa), RBOHD/C was divided into three overlapping
186 fragments (C1, C2, and C3; Fig. 3d). The results showed that the C1 and C3 fragments of 6His-MBP-
187 RBOHD were preferentially phosphorylated by 6His-GST-CRK2_{cyto} while C2 displayed considerably
188 weaker phosphorylation (Fig. 4b). Mass spectrometric analysis of in-gel trypsin- or Lys-C-digested peptides
189 identified *in vitro* RBOHD phosphorylation sites targeted by CRK2_{cyto} (Table S1). In the N-terminal region
190 of RBOHD two sites targeted by CRK2 were identified (S8 and S39), while three sites (S611, S703, S862)
191 were identified in the C-terminal region. Taken together our results show that the N- and C-terminal regions
192 of RBOHD are phosphorylated by CRK2 *in vitro*.

193 **CRK2 regulates RBOHD via phosphorylation of S703 and S862**

194 Among the RBOHD phospho-sites targeted by *in vitro* phospho-sites S8 and S39 have been previously
195 described to be phosphorylated by SIK1¹⁰ and BIK1^{11,12}. S703 has been reported to be phosphorylated upon
196 xylanase treatment but no responsible kinase was identified³⁴ while phosphorylation of S611 and S862 has
197 not been described so far. In order to test whether the identified phospho-sites in RBOHD were important for
198 the regulation of RBOHD activity, the residues S8, S39, S611, S703, and S862 were substituted with alanine
199 to make them non-phosphorylatable. Wild type RBOHD and phospho-site mutant constructs were
200 transfected into HEK293T cells together with CRK2. Amino acid substitutions did not affect RBOHD
201 protein levels (Fig. S5a and S5b). Substitution of S8 or S39 in the N-terminal cytoplasmic region of RBOHD
202 did not impact ROS-producing activity compared to the wild type protein when co-transfected with CRK2
203 (Fig. 5a). The 3FLAG-RBOHD^{S703A} and CRK2-3Myc co-transfected cells showed reduced basal ROS
204 production as compared to 3FLAG-RBOHD and CRK2-3Myc, (Fig. 5b), suggesting that S703 could be a
205 positive regulatory site for RBOHD activity. In contrast to 3FLAG-RBOHD^{S703A}, HEK293T cells expressing
206 3FLAG-RBOHD^{S862A} and CRK2-3Myc exhibited higher basal ROS production compared to 3FLAG-
207 RBOHD and CRK2-3Myc (Fig. 5b), suggesting that S862 could act as a negative regulatory site. ROS
208 production of 3FLAG-RBOHD^{S611A} co-transfected with CRK2-3Myc was similar to 3FLAG-RBOHD
209 suggesting no regulatory role of this single site. Mutation of S703 or S862 of RBOHD did not impair Ca²⁺-
210 dependent activation of ROS production (Figs. S5c and S5d). Taken together, our results suggest that the
211 phospho-sites in the C-terminal cytoplasmic region of RBOHD could be crucial for fine-tuning ROS
212 production activity.

213 **Phosphorylation of S703 and S862 of RBOHD modulates flg22-induced ROS production in planta**

214 To investigate whether RBOHD phosphorylation sites targeted by CRK2 *in vitro* were also phosphorylated
215 upon flg22-treatment *in planta*, we carried out targeted phosphoproteomic analyses of Col-0 plants treated
216 with flg22 for 5 min. Phosphorylation of S8 was not significantly induced by flg22-treatment (Fig. 6a, S6a
217 and b) while S39 phosphorylation was strongly enhanced (Fig. 6b and S6c). Phosphorylation of S703, which
218 was targeted by CRK2 *in vitro* and mutation to alanine reduced ROS production, was significantly enhanced
219 upon flg22 treatment (Fig. 6c and Fig. S6d). As previously shown, phosphorylation of S163, S343 and S347
220 in RBOHD (Fig. S6e-g) as well as dual phosphorylation of the TEY-motif in the MAPKs MPK3, MPK6 and
221 MPK11 (Fig. S7h-j) were enhanced by flg22-treatment³⁵. Phosphorylation of S611 could not be evaluated as
222 trypsin or Lys-C digestion resulted in an inappropriate length of peptides that contain the phospho-sites for
223 LC-MS-based targeted analyses. Phosphorylation of S862 could not be investigated since digestion with both
224 trypsin and Lys-C resulted in a peptide too short for analysis and not specific for RBOHD. In summary, our
225 results suggest that phosphorylation of S703 in the C-terminus of RBOHD is important for full flg22-
226 triggered ROS production also *in planta*.

227 To investigate whether phosphorylation of S703 or S862 in the C-terminal region of RBOHD also impacts
228 RBOHD-dependent ROS production *in planta*, we generated transgenic plants expressing RBOHD,

229 RBOHD^{S703A} or RBOHD^{S862A} under the control of the *RBOHD promoter* (*RBOHDpro::3FLAG-RBOHD*) in
230 *rbohD* background. The phospho-site mutations did not alter growth or development compared to the
231 3FLAG-RBOHD expressing plants (Fig. S7a). Lines expressing similar amounts of 3FLAG-RBOHD,
232 3FLAG-RBOHD^{S703A} or 3FLAG-RBOHD^{S862A} were selected for further analysis (Figs. S7b and c).
233 Compared with 3FLAG-RBOHD expression lines, flg22-triggered ROS production in 3FLAG-RBOHD^{S703A}
234 lines was significantly reduced (Figs. 6d and S7d) and the ROS production in 3FLAG-RBOHD^{S862} lines were
235 enhanced (Figs. 6e and S7e).

236 **C-terminal phosphorylation sites are conserved in plant and animal NADPH oxidases**

237 Since little is known about regulation of RBOH activity *via* its C-terminus we investigated whether
238 regulation through S703 or S862 was unique to RBOHD or conserved also in other RBOHs. We constructed
239 a phylogenetic tree of RBOHs from plant genomes representing major branches of the plant lineages (Fig. 7).
240 Plant RBOHs form a monophyletic group, which is separated from human NOX2 and NOX5. The sequence
241 context of S8 and S39 is poorly conserved outside the clade containing RBOHD from Arabidopsis
242 suggesting that the N-terminal region has experienced considerable changes during the evolution of the
243 RBOH protein family (Fig. 7). In contrast to the N-terminal region, the phospho-sites in the C-terminal
244 region displayed strong conservation throughout the plant RBOH clade. S703 was conserved in a
245 monophyletic clade containing eight of the ten RBOHs from Arabidopsis but not in the clade containing
246 RBOHH and RBOHJ (Fig. 7). The phospho-sites S611 as well as S862, which has a putative negative
247 regulatory function, were strongly conserved in all plant RBOHs. The sequence motifs harboring S611 and
248 S862 are intriguingly conserved even in human NOX2 and NOX5 (Fig. 7). Since the C-terminal region binds
249 FAD and NADPH its evolution may underlie stricter evolutionary constraints compared to the N-terminal
250 region. Remarkably, even phospho-sites and their sequence context in the C-terminal region are conserved in
251 NADPH oxidases from plants and animals.

252 Discussion

253 CRKs are a large group of RLKs involved in biotic and abiotic stress signaling in Arabidopsis²⁵. We have
254 previously shown that flg22-triggered extracellular ROS production is altered in several *crk* mutants²⁵. In
255 particular CRK2, a member of the basal clade of CRKs²¹, has been highlighted since *crk2* displays striking
256 phenotypes²⁵ including reduced rosette size and reduced flg22-induced ROS production. Functional CRK2
257 restored the growth defect (Fig. 1) as well as the MAMP-induced ROS burst (Fig. 2). In addition to their role
258 in stress responses, extracellular ROS have also been implicated in leaf cell expansion³⁶, and the *rboh*d and *f*
259 double mutant displays reduced rosette size⁶. Overexpression of CRKs has been associated with increased
260 SA accumulation^{26,28}. However, since SA levels were unaltered in the loss-of-function mutant *crk2*, its
261 smaller size may be a consequence of impaired ROS production (Fig. S1b). Alternatively, other substrates of
262 CRK2 might be involved in the regulation of plant growth. This is supported by the observation that CRK2
263 enhanced the activity of RBOHD but also RBOHF in HEK293T cells (Fig. S3d and S3f). In line with
264 reduced MAMP-induced ROS production, *crk2* was more susceptible to the virulent bacterial pathogen *Pto*
265 DC3000 (Fig. 2) suggesting that CRK2-mediated ROS production was essential to effectively counter
266 pathogen infection. Also other flg22-induced defense responses were altered in *crk2* including reduced
267 changes in cytosolic Ca²⁺ but enhanced callose deposition and MAPK activation (Fig. 2d, 2e, and S2e-S2g).
268 Ca²⁺ is important for the activation of RBOH but ROS also triggers Ca²⁺ fluxes in plants¹. Thus, the
269 diminished increase of cytosolic Ca²⁺ in *crk2* may be a consequence of the impaired flg22-induced ROS
270 production. Also, callose deposition^{37,38} has been previously linked to ROS production²⁰ and CRK2 interacts
271 with callose synthases and phosphorylates CALLOSE SYNTHASE 1 (CALS1) *in vitro*³¹. However, unlike
272 in the response to flg22, salt-induced callose deposition is reduced in *crk2*³¹ suggesting that CRK2 might
273 regulate different callose synthases in response to biotic and abiotic stimuli. Interestingly, CRK2 forms
274 clusters at the plasma membrane in response to flg22-treatment and ROS is required for this process³¹. It is
275 not clear how these clusters are integrated with the regulation of RBOHD activity but it might serve to
276 connect RBOHD-dependent ROS production with callose deposition. Another important element in response
277 to biotic and abiotic cues^{39,40} is the activation of MAPK cascades and earlier reports suggest a bifurcation of
278 defense signaling following MAMP-perception. CRK2 could be involved in balancing MAMP-induced ROS
279 signaling pathways and MAPK signaling but the mechanism is still unclear. Thus, CRK2 likely participates
280 in the control of ROS production *via* interaction with RBOHD rather than MAMP-receptor complexes.
281 Intriguingly, CRK2 existed in a pre-formed complex with RBOHD *in planta* independent of MAMP-
282 treatment (Fig. 3) while many other RLK protein complexes are formed upon signal perception.

283 Phosphorylation of the C-terminus is a critical for the regulation of human NADPH oxidases.
284 Phosphorylation of the NOX2 C-terminus by protein kinase C (PKC) enhances assembly of the multimeric
285 NOX2 complex and its activity, whereas phosphorylation by *ataxia telangiectasia*-mutated (ATM) kinase
286 inhibits NOX2 activity^{17,41}. NOX5 activity is regulated by Ca²⁺-binding to EF-hands in the N-terminus⁴² but
287 NOX5 is also activated by phosphorylation of the C-terminus by PKC α or calcium/calmodulin-dependent

288 kinase II (CAMKII)^{43,44}. Although the C-terminal catalytic domain of RBOHs is highly conserved, the N-
289 terminus has been considered as important for activation of the ROS-production activity and multiple
290 phospho-sites (S8, S39, S133, S148, S163, S339, S334 and S347) have been reported. Intriguingly,
291 CRK2_{cyto} interacted with and phosphorylated the C-terminal region at S611, S703 and S862 (Fig. 3 and
292 Table S1). Phosphorylation of S703 has been reported³⁴ but not linked with modulation of ROS production.
293 Mutation S703A in the C-terminus of RBOHD led to reduced CRK2-dependent RBOHD activity in
294 HEK293T cells and reduced flg22-induced ROS production *in planta*, while the S862A mutation resulted in
295 enhanced ROS production (Fig. 5 and 6). These results suggest that CRK2-mediated phosphorylation of the
296 RBOHD C-terminus at S703 and S862 likely contributes to the regulation of MAMP-induced regulation
297 ROS production. Phosphorylation sites in the N-terminus of plant RBOHs showed only moderate
298 conservation (Fig. 7) likely reflecting functional diversification. By contrast, phosphorylation sites in the C-
299 terminus were highly conserved among RBOHs (Fig. 7) suggesting that phosphorylation of the C-terminal
300 region could be a general feature of plant NADPH oxidases. Remarkably, two putative RBOHD phospho-
301 sites, S611 and S862, were identified even in the human NADPH oxidases NOX2 and NOX5 (Fig. 7).
302 RBOHD can also be regulated by cysteine S-nitrosylation in the C-terminus⁴⁵ but it is unclear how this
303 modification is integrated with other regulatory mechanisms. Taken together, our results suggest that
304 phosphorylation of the C-terminal region of plant NADPH oxidases is strongly conserved and important for
305 controlling ROS production.

306 Several protein kinases phosphorylate RBOHD N-terminus and regulate the activity including RLCKs^{11,12,46},
307 MAP4Ks¹⁰, CPKs¹³ and RLKs⁴⁷ but how is regulation by phosphorylation of the N- and C-terminal regions
308 coordinated? BIK1 is a component involved in the activation of RBOHD by phosphorylation^{11,12} and ROS
309 production in *bik1* is reduced to a similar extent as in *crk2*. However, reduced flg22-induced ROS production
310 in *crk2* was not due to lower *BIK1* transcript abundance (Fig. S8). *BIK1* homologs, AvrPphB
311 SUSCEPTIBLE1 (PBS1) and AvrPphB SUSCEPTIBLE1-LIKE (PBL) kinases, contribute to the regulation
312 of RBOH activity and ROS production is progressively reduced in double mutants with *bik1*^{46,48}. CRK2 and
313 BIK1 could synergistically regulate ROS production but we were unable to obtain a double mutant between
314 *bik1* and *crk2* (Table S2). Therefore, we propose that at least one of these components is essentially required.
315 BIK1 has previously been shown to interact with other kinases including CRKs⁴⁹ but interaction with CRK2
316 has not been investigated. BIK1 and CRK2 are likely highly coordinated in order to precisely control ROS
317 production in response to environmental stimuli (Fig 8). Like CRKs, RBOHs are involved in diverse
318 processes in stress responses and also plant development, for example AtRBOHH and J are important for
319 pollen tube growth⁵⁰. Two CRKs are predominantly expressed in pollen. CRK1 and CRK46 are close
320 homologs of CRK2 and it is conceivable that they regulate RBOHH and J, potentially *via* phosphorylation of
321 the C-terminal region.

322 In summary, we propose that CRK2 is a central element in orchestrating the extracellular ROS burst and in
323 mediating the balance between different defense responses. The full complexity and integration of the

324 regulatory components controlling RBOH activity is still a topic of much speculation¹. The diversity of
325 regulators converging at RBOHs reflects the prominent role of apoplastic ROS in signal transduction while
326 simultaneously strict control is required to circumnavigate oxidative damage. We suggest that RBOHD is
327 regulated by phosphorylation of the C-terminal region to complement regulatory mechanisms targeting the
328 N-terminus (Fig. 8). The conservation of serine and threonine residues in the C-terminus of NADPH
329 oxidases suggests that this mode of regulation is evolutionarily conserved in plants and animals. In the future
330 it will be interesting to investigate how CRK-mediated phosphorylation of the RBOH C-terminus is
331 integrated in the diverse processes which incorporate extracellular ROS.

332 **Materials and methods**

333 **Plant Material and growth condition**

334 *Arabidopsis thaliana* plants used in this study include Col-0, *crk2*²⁵, *rbohD*⁶, *fls2*⁵¹, *bik1*⁵² and 35S::FLAG-
335 *RBOHD/rbohD*¹¹. To generate *crk2/bik1* double mutant, *crk2* and *bik1* single mutant plants were crossed. F1,
336 F2 and F3 progenies were analyzed by PCR. F2 and F3 seeds were obtained by self-pollination. Primers are
337 listed in Table S3.

338 Seeds were sterilized by 70 % ethanol 2 % Triton X-100 for 5 min and washed 3 times with 99 % ethanol.
339 Surface sterilized seeds were sown on 1x or ½ strength Murashige and Skoog (MS) medium containing 1 %
340 sucrose and subsequently stratified for 2-4 days in the dark at 4 °C. Plants were grown in growth chambers
341 (Panasonic, #MLR-352-PE) under 12 h light/12 h dark (22°C /18°C). After 10 days, seedlings were
342 transferred to soil and grown in growth rooms under the following conditions: 12 h light/12 h dark (23 °C
343 /19 °C), relative humidity 50-60 %, unless otherwise stated.

344 For SA measurements seedlings were grown in liquid culture as described⁵³ with minor modifications. 20 mg
345 of seeds were sterilized by sequential incubation with 70 % ethanol and 50 % bleach on a rotating mixer for
346 10 min each and washed three times with sterile water. Seeds were then transferred into 250 mL Erlenmeyer
347 flasks containing 125 mL ½ strength MS medium supplemented with 1 % sucrose. Seedlings were grown
348 under long-day conditions (16 h light /8 h dark, 22 °C/18 °C) at 150 μmol m⁻² s⁻¹ photon flux density on an
349 IKA KS501 flask shaker at a constant speed of 130 rotations per minute. Seedlings were collected after 6
350 days of growth.

351 *Nicotiana benthamiana* plants were grown in the greenhouse under 18 h light/6 h dark (23 °C /19 °C).

352 **Cell culture and Transfection**

353 HEK293T cells (ATCC, #CRL-3216) were maintained at 37 °C in 5 % CO₂ in Dulbecco's Modified Eagle's
354 Medium nutrient mixture Ham's F-12 (SIGMA, #D8062) supplemented with 10 % fetal bovine serum
355 (Gibco, #26140-079). Cells were transfected with *pcDNA3.1* and *pEFI* vectors using GeneJuice transfection
356 reagent (Merck Millipore, #70967-3) according to the manufacturer's instructions.

357 **Plasmid construction**

358 *CRK2* and *RBOHD* constructs for *Arabidopsis* were generated through MultiSite Gateway technology
359 (Invitrogen). To generate pBm43GW-CRK2pro::CRK2-Venus (YFP)-3AT for *crk2* complementation lines,
360 the coding region of *CRK2* or kinase-dead mutants (K353E or D450N) were recombined into pENTR/D-
361 TOPO vector (Invitrogen). pDONRP4P1R/zeo-CRK2pro, pDONR/zeo-CRK2 (or pENTR/D-TOPO-CRK2
362 kinase-dead mutant) and p2R3a-VenusYFP-3AT were recombined with pBm43GW. To generate
363 pHm43GW-pRBOHD::3FLAG-RBOHD-nosT, the coding region of 3FLAG-RBOHD was amplified by
364 PCR from pcDNA3.1-3FLAG-RBOHD and cloned into pDONR/zeo vector (Invitrogen). The promoter
365 region of *RBOHD* was amplified by PCR from pBin19g-pRBOHD::3FLAG-RBOHD and cloned into

366 pDONRP4P1R/zeo vector (Invitrogen). pDONRP4P1R/zeo-RBOHDpro, pDONR/zeo-3FLAG-RBOHD and
367 p2R3a-nosT were recombined with pHm43GW. Single amino acid substitution mutants of *CRK2* and
368 *RBOHD* were generated by point-mutant primers and the mega-primer PCR method. pBm43GW-
369 CRK2pro::CRK2-YFP-3AT and pHm43GW-pRBOHD::3FLAG-RBOHD-nosT constructs were transformed
370 into *crk2* and *rbohD* plants, respectively, by *Agrobacterium tumefaciens* strain GV3101 (pSoup)-mediated
371 floral dipping⁵⁴. To generate *CRK2* over-expression lines for co-immunoprecipitation, pBm43GW-
372 35S::CRK2-YFP-3AT were transformed into Col-0. p2R3a-Venus(YFP)-3AT, p2R3a-nosT, pBm43GW and
373 pHm43GW⁵⁵, pBin19g-pRBOHD::3FLAG-RBOHD¹¹, pDONR/zeo-CRK2 and pBm43GW-35S::CRK2-
374 YFP-3AT³¹, pDONRP4P1R/zeo-CRK2pro³¹, pcDNA3.1-3FLAG-RBOHD⁹ have been described previously.

375 For BiFC assays, the pDOE-07 vector⁵⁶ MCS3 was mutagenized (pDOE-07m) as described before⁵⁷. To
376 generate the NmVen210::RBOHD – CRK2::CVen210 construct, the coding regions of RBOHD and CRK2
377 were amplified by PCR, and inserted between *Bam*HI and *Spe*I in MCS1 and between *San*DI and *Sna*BI sites
378 in MCS3 of pDOE-07m, respectively. To generate NmVen210::RBOHD – GUS::CVen210 construct, the
379 fragments RBOHD and GUS (β -glucuronidase *uidA*) were amplified by PCR, and inserted between *Asc*I and
380 *Spe*I sites in pDOE-07m MCS1 and between *San*DI and *Pml*I sites in MCS3 of pDOE-07m, respectively.

381 6His-GST-CRK2cyto and 6His-MBP-RBOHD/C constructs for recombinant proteins were generated by
382 using In-Fusion technology (Clontech). The coding regions of CRK2cyto (WT, K353E, and D450N),
383 RBOHD/C (full-length, C1, C2, and C3) were amplified by PCR and cloned into pOPINK (Addgene,
384 #41143) or pOPINM (Addgene, #26044) vectors. pOPINM-RBOHD/N was described previously¹¹. To
385 generate the GST-BIK1 construct, BIK1 fragment was cloned into the *Bam*HI and *Not*I sites of pGEX6P-1
386 (GE Healthcare).

387 For HEK293T cell experiments, pEF1-MCS-3Myc [*Bam*HI-*Not*I-3Myc-stop fragment was inserted between
388 *Kpn*I and *Xba*I sites of pEF1/myc-His B vector (Invitrogen)] was generated. To generate pEF1-CRK2 (WT
389 or D450N)-3Myc, the codon optimized coding sequence of Kozak-CRK2 (WT or D450N) was cloned
390 between *Bam*HI and *Not*I sites of pEF1-MCS-3Myc. To generate pcDNA3.1-3FLAG-RBOHD mutant
391 constructs, the coding regions of RBOHD (S8A, S39A, S611A, S703A, or S862A) were cloned into *Bam*HI
392 site of pcDNA3.1-3FLAG-MCS [Kozak-3FLAG-*Bam*HI-EcoRV-stop fragment was inserted between *Nhe*I
393 and *Kpn*I sites of pcDNA3.1(-) vector (Invitrogen)]. Amino acid substituted mutants of CRK2 and RBOHD
394 were generated by point-mutant primers and the mega-primer PCR method. pEF1-3Myc-GFP⁵⁸, pcDNA3.1-
395 3FLAG-RBOHD, pcDNA3.1-3FLAG-RBOHC, pcDNA3.1-3FLAG-RBOHF and pcDNA3.1-3FLAG-MCS
396 were described previously⁹. Primer sequences are listed in the Table S3.

397 **Subcellular protein localization and BiFC observation**

398 Fluorescent images were obtained using a Leica TCS SP5 II HCS confocal microscope. For investigation of
399 CRK2-YFP localization, 514 nm excitation and 525-590 nm detection range were used. For BiFC assays, the

400 mTq2 was excited at 458 nm and a detection range of 480-520 nm; mVenus was excited at 514 nm excitation
401 and detected using a range of 525-575 nm. Chlorophyll autofluorescence was excited at 458 nm and detected
402 using a range of 650-710 nm.

403 **ROS measurements**

404 Leaf discs were collected using a cork borer from 4-week-old *Arabidopsis* plants and floated overnight in
405 sterile distilled water in 96 well plates under continuous light at room temperature. On the following day,
406 water was replaced with assay buffer containing 34 mg/L luminol sodium salt (Sigma, #A4685), 20 mg/L
407 horse radish peroxidase (Fujifilm Wako, #169-10791), 200 nM flg22 (GenScript), 200 µg/mL Chitin (Sigma,
408 #C9752) or 1 µM AtPep1 (ATKVKAKQRGKEKVSSGRPGQHN: synthesized by Synpeptide, China).
409 Luminescence was measured for 1 sec every 1 min at room temperature using GloMax-Multi+Detection
410 System (Promega). ROS production was expressed in relative luminescence units (RLU).

411 The ROS producing activity of RBOHs in HEK293T cells was measured as described previously¹⁵. Two
412 days after transfection, medium was removed and cells were gently washed with 1xHBSS (GIBCO, #14025-
413 092 or #14175-095). Measurements were started after addition of the assay buffer containing 250 µM
414 luminol sodium salt and 66.7 mg/L horse radish peroxidase. After 30 min measurement, 1µM ionomycin
415 (Calbiochem, #407952) was added. Chemiluminescence was measured for 1 sec every 1 min at 37 °C using
416 GloMax-Multi+Detection System. ROS production was expressed in relative luminescence units (RLU).
417 Expressed proteins were detected by immunoblotting with anti-FLAG (Sigma, #F1804), anti-cMyc (Fujifilm
418 Wako, #017-2187), anti-β-actin (Sigma, #A5316) and IRDye800CW anti-mouse IgG (LI-COR, #926-32210)
419 antibodies.

420 **Bacterial growth assay**

421 To quantify bacterial growth on 4-week-old plants infected with the virulent *Pto*DC3000⁵⁹, growth curve
422 assays were performed as described previously⁶⁰.

423 **Ca²⁺ imaging**

424 Calcium imaging with YCNano-65 expressing plants was performed as described previously³¹. 7-day-old
425 seedlings were mounted and 1 µL of 200 nM flg22 was applied to the adaxial surface of cotyledons.

426 **MAPK assay**

427 MAPK assays were performed as previously described²⁴. In brief, 4-week-old *Arabidopsis* plants were
428 sprayed with 10 µM flg22 with 0.025 % Silwet L-77. Leaf samples were ground in liquid nitrogen and sand.
429 Extraction buffer [50 mM HEPES (pH7.4), 50 mM NaCl, 10 mM EDTA, 0.2 % Triron X-100, 1 % Protease
430 inhibitor cocktail (SIGMA, #P9599), 1 % Halt phosphatase inhibitor cocktail (Thermo scientific, #78428)]
431 was added (2 mL/g plant powder). Samples were incubated at 4 °C for 30 min and centrifuged at 12,000 x g,
432 4 °C for 10 min. The supernatant was used for immunoblotting with anti-Phospho-p44/42 MAPK (Cell
433 Signaling Technology, #4370) and IRDye800CW anti-rabbit IgG (LI-COR, #926-32211) antibodies.

434 **Callose Staining**

435 Callose staining was performed as described previously³¹.

436 **qRT-PCR**

437 Col-0, *crk2* and *fls2* seedlings were grown on MS 1 % sucrose agar plate for 5 days and were transferred into
438 MS 1 % sucrose liquid media and grown for 5 days. Plants were incubated with 1 μ M flg22 for 30 min, 1 h
439 and 3 h, respectively. Plants were ground in liquid nitrogen and total RNA was extracted using the GeneJET
440 Plant RNA purification Kit (Thermo scientific, #K0802). Total RNA was treated with DNase I (Thermo
441 scientific, #EN0525) and cDNA was synthesized with Maxima H Minus Reverse Transcriptase (Thermo
442 scientific, #EP0751). qPCR analysis was performed with CFX real-time PCR (BioRad, Hercules, CA, US)
443 using 5 \times HOT FIREPol EvaGreen qPCR Mix Plus ROX (Soils Biodyne). *SAND*, *TIP41* and *YLS8* were used
444 as reference genes for normalization. Relative expression was calculated with qBase+
445 (Biogazelle; <https://www.qbaseplus.com/>). Primers are listed in Table S3.

446 **Phytohormone analysis**

447 SA was analyzed from liquid-cultured seedlings as described previously⁶¹ with minor modifications.
448 Seedlings were flash-frozen in liquid nitrogen and freeze-dried for 24 h. About 6 mg aliquots of freeze-dried
449 material were homogenized by shaking with 5 mm stainless steel beads in a Qiagen Tissue Lyser II for 2 min
450 at 25 Hz. Shaking was repeated after addition of 400 μ L extraction buffer (10 % methanol, 1 % acetic acid)
451 with internal standard (28 ng Salicylic-d₄ Acid; CDN Isotopes, Pointe-Claire, Canada). Samples were then
452 incubated on ice for 30 min and centrifuged for 10 min at 16,000 x g and 4 °C. Supernatants were transferred
453 into fresh 2 mL tubes and pellets were re-extracted with 400 μ L extraction buffer without internal standards.
454 Supernatants were combined and centrifuged 3 times to remove all debris before LC-MS/MS analysis.

455 The chromatographic separation was carried out using an Acquity UHPLC Thermo system
456 (Waters, Milford, U.S.) equipped with a Waters Cortecs C18 column (2.7 μ m, 2.1 x 100 mm). The solvent
457 gradient (acetonitrile (ACN) / water with 0.1 % formic acid each) was adapted to a total run time of 7 min: 0-
458 4 min 20 % to 95 % ACN, 4-5 min 95 % ACN, 5-7 min 95 % to 20 % ACN; flow rate 0.4 mL / min. For
459 hormone identification and quantification, a tandem mass spectrometric system Xevo TQ-
460 XS, triple quadrupole mass analyser (QqQ) with a ZSpray ESI function (Waters, Milford, U.S.) was used.
461 Mass transitions were: SA 137 > 93, D₄-SA 141 > 97.

462 **Protein extraction and Co-immunoprecipitation**

463 Co-immunoprecipitation was performed as described previously⁶². Homozygous *35S::FLAG-RBOHD/rbohD*
464 was crossed with homozygous *35S::CRK2-YFP/Col-0* or *35S::YFP-6Myc/Col-0*. *35S::FLAG-*
465 *RBOHD/35S::CRK2-YFP/rbohD* F3 plants were selected by kanamycin resistance (homozygous FLAG-
466 RBOHD insertion) and PCR (homozygous *rbohD* T-DNA insertion). F1 and F3 plants were grown on MS
467 1 % sucrose agar plate for 7 days and were transferred into MS 1 % sucrose liquid media and grown for 8-10
468 days. F3 plants were incubated in water or 1 μ M flg22 for 10 min or 30 min after vacuum application for 2

469 min. Plants were ground in liquid nitrogen and sand. Extraction buffer [50 mM Tris-HCl (pH 7.5), 150 mM
470 NaCl, 10 % Glycerol, 5 mM DTT, 1 % Protease inhibitor cocktail (SIGMA, P9599), 2 % IGEPAL CA630, 1
471 mM Na₂MoO₄·2H₂O, 2.5 mM NaF, 1.5 mM Activated sodium orthovanadate, 1 mM PMSF] was added at
472 1.5 - 2 mL/g fresh weight. Samples were incubated at 4 °C for 1 h and centrifuged at 15,000 x g, 4 °C for 20
473 min. Supernatants were adjusted to 5 mg/mL protein concentration and incubated for 1 h at 4 °C with 100 µL
474 of anti-GFP magnetic beads (Miltenyi Biotec, #130-091-125). Bound proteins were analyzed by
475 immunoblotting with anti-GFP (Invitrogen, #A11122), anti-RBOHD (Agrisera, #AS15-2962), and
476 IRDye800CW anti-rabbit IgG (LI-COR, #926-32211) antibodies.

477 To detect 3FLAG-RBOHD, total protein was extracted from *RBOHDpro::3FLAG-RBOHD* (WT, S703A and
478 S862A)/*rbohD* T3 homozygous plants with the same extraction buffer and analyzed by immunoblotting with
479 anti-FLAG (Sigma, #F1804 and IRDye800CW anti-mouse IgG (LI-COR, #926-32210) antibodies.

480 **BiFC assay**

481 *Agrobacterium tumefaciens* strain GV3101 (pSoup) containing the binary plasmid was grown in LB medium
482 with appropriate antibiotics at 28 °C overnight. The cells were washed once in infiltration buffer [10 mM
483 MES, 10 mM MgCl₂, 200 µM acetosyringone], and resuspended to a final OD₆₀₀ of 1.0. After incubation on
484 ice for 1 h, 6-week-old *Nicotiana benthamiana* plants were inoculated with a 1 mL needleless syringe.
485 Leaves were observed at 2-day post-inoculation.

486 **Protein purification from *E.coli***

487 Cytosolic regions of CRK2 were expressed in *Escherichia coli* Lemo21. Cytosolic regions of RBOHD, BIK1
488 and MBP were expressed in *Escherichia coli* BL21. Glutathione S transferase (GST)-tagged recombinant
489 proteins were purified using glutathione sepharose 4B (GE Healthcare, #17-0756-01) according to
490 manufacturer's instructions. Maltose binding protein (MBP)-tagged proteins were purified using amylose
491 resin (New England Biolabs, #E8021S) according to manufacturer's instructions.

492 ***In vitro* pull down**

493 6His-GST-CRK2_{cyto}, 6His-MBP-RBOHD/N, 6His-MBP-RBOHD/C and MBP were incubated with
494 glutathione Sepharose 4B in the pull down buffer (20 mM HEPES, 50 mM KCl, 5 mM NaCl, 1 % Tween20,
495 1 mM DTT and 100 µM PMSF) at 4 °C for 1 h. The glutathione sepharose 4B was washed four times with
496 the pull down buffer and eluted with 10 mM reduced glutathione. The mixture was analyzed by
497 immunoblotting anti-6xHis (Invitrogen, #MA1-135), anti-MBP (Santa Cruz Biotechnology, #sc-13564) and
498 IRDy800CW anti-mouse IgG antibodies.

499 ***In vitro* kinase assay**

500 Purified recombinant proteins were incubated with [γ-³²P] for 30 min at room temperature in the kinase assay
501 buffer [50 mM HEPES (pH7.4), 1 mM DTT, 10 mM MgCl₂, 0.6 mM unlabeled ATP]. The mixture was
502 subsequently separated by SDS-PAGE and autoradiography was detected by FLA-5100 image analyzer

503 (Fujifilm, Japan). For identification of *in vitro* phosphorylation sites by LC-ESI-MS/MS, 1.5 mM unlabeled
504 ATP was used in the kinase buffer. The proteins were separated by SDS-PAGE, followed by CBB staining
505 and were digested by trypsin (Thermo scientific, #90057) or Lys-C (Thermo scientific, #90051).

506 **Identification of *in vitro* phosphorylation sites of RBOHD by LC-ESI-MS/MS**

507 Trypsin or Lys-C digested protein samples were analyzed by a Q Exactive mass spectrometer (Thermo
508 Fisher Scientific, Bremen, Germany) connected to Easy NanoLC 1000 (Thermo Fisher Scientific). Peptides
509 were first loaded on a trapping column and subsequently separated inline on a 15 cm C18 column (75 μm x
510 15 cm, ReproSil-Pur 5 μm 200 Å C18-AQ, Dr. Maisch HPLC GmbH, Ammerbuch-Entringen, Germany).
511 The mobile phase consisted of water with 0.1 % formic acid (solvent A) or acetonitrile/water [80:20 (v/v)]
512 with 0.1 % formic acid (solvent B). A linear 10 min gradient from 8 % to 42 % B was used to elute peptides.

513 MS data was acquired automatically by using Thermo Xcalibur 3.1 software (Thermo Fisher Scientific). An
514 information dependent acquisition method consisted of an Orbitrap MS survey scan of mass range 300-2000
515 m/z followed by HCD fragmentation for 10 most intense peptide ions. Raw data was searched for protein
516 identification by Proteome Discoverer (version 2.2) connected to in-house Mascot (v. 2.6.1) server.
517 Phosphorylation site locations were validated using phosphoRS algorithm. A SwissProt database with a
518 taxonomy filter *Arabidopsis thaliana* was used. Two missed cleavages were allowed. Peptide mass tolerance
519 ± 10 ppm and fragment mass tolerance ± 0.02 Da were used. Carbamidomethyl (C) was set as a fixed
520 modification and methionine oxidation, acetylation of protein N-terminus, phosphorylation of Ser and Thr
521 were included as variable modifications. Only peptides with FDR 0.01 were used.

522 **Targeted (phospho) peptide analysis**

523 **Plant treatment and phosphopeptide enrichment.** Arabidopsis seeds were sterilized by incubating with
524 1.5 % NaClO 0.02 % Triton X-100 solution for 5 min and vernalized at 4 °C for 2 days. Sterilized seeds
525 were germinated and grown in liquid culture on 6 well plates (30 seeds/well) in MGRL medium with 0.1 %
526 (w/v) sucrose (2 mL/well)⁶³ at 23 °C under continuous light (100 $\mu\text{mol m}^{-2} \text{s}^{-1}$) in a Percival growth chamber.
527 Plates with 11-day-old seedlings were transferred from the growth chamber to a workbench and kept o/n for
528 acclimatization before treatments. Seedlings were treated with either 1 μM flg22 or sterile water for 5 min
529 after which seedlings were immediately collected and flash-frozen in liquid nitrogen and stored at -80 °C.
530 Frozen seedlings were disrupted using a Retsch mill (5 min, 30 Hz), and 500 μL urea extraction buffer [8M
531 urea in 100mM Tris, pH 8.5, 20 $\mu\text{L}/\text{mL}$ Phosphatase Inhibitor Cocktail 3 (Sigma, P0044), 20 $\mu\text{L}/\text{mL}$
532 Phosphatase Inhibitor Cocktail 2 (Sigma, P5726), 5 mM DTT] was added to the disrupted frozen powders,
533 mixed briefly and incubated at RT for 30 min. After centrifugation at 15,000 x g for 10 min, supernatants
534 were transferred to fresh tubes. Protein concentrations were determined using Pierce 660 nm protein assay
535 (Thermo Scientific). Extracts with 500 μg of protein were alkylated with 14 mM chloroacetamide (CAA) at
536 RT for 30 min in the dark, CAA was quenched by addition of 1/200 sample volume 1M DTT. Samples were
537 diluted 1:8 with 0.1 M Tris, pH 8.5, 1 mM CaCl_2 and were digested o/n at RT either with 5 μg trypsin or 5

538 μ g Lys-C. Digestion reaction was terminated by addition of TFA (0.1 % final concentration), and peptides
539 were desalted using C18 SepPaks [1cc cartridge, 100 mg (WAT023590)]. In brief, SepPaks were
540 conditioned using methanol (1 mL), buffer B (80 % acetonitrile, 0.1 % TFA; 1 mL) and buffer A (0.1 %
541 TFA; 2 mL). Samples were loaded by gravity flow, washed with buffer A (1 x 1 mL, 1 x 2 mL) and eluted
542 with buffer B (2 x 400 μ L). 40 μ L of eluates were kept separately to measure non-phosphopeptides and the
543 rest were used for further phosphopeptide enrichment. Phosphopeptide enrichment was performed by
544 hydroxy acid-modified metal-oxide chromatography (HAMMOC) using titania as described previously with
545 minor modifications^{64,65}.

546 **LC-MS/MS data acquisition.** Samples were analyzed using an EASY-nLC 1200 (Thermo Fisher) coupled
547 to a Q Exactive Plus mass spectrometer (Thermo Fisher). Peptides were separated on 16 cm frit-less silica
548 emitters (New Objective, 0.75 μ m inner diameter), packed in-house with reversed-phase ReproSil-Pur C18
549 AQ 1.9 μ m resin (Dr. Maisch). Peptides were loaded on the column and eluted for 115 min using a
550 segmented linear gradient of 5 % to 95 % solvent B (0 min, 5 % B; 0-5 min, 5 % B; 5-65 min, 20 % B; 65-90
551 min, 35 % B; 90-100 min, 55 % B; 100-105 min, 95 % B; 105-115 min, 95 % B) [solvent A (0 % ACN,
552 0.1 % FA); solvent B (80 % ACN, 0.1 % FA)] at a flow rate of 300 nL/min. Mass spectra were acquired
553 using a targeted (parallel reaction monitoring, PRM) approach. The acquisition method consisted of a full
554 scan method combined with a non-scheduled PRM method. The 16 targeted precursor ions were selected
555 based on the results of a DDA peptide search of phospho-enriched samples in Skyline⁶⁶ (Version 4.2.0.x,
556 <https://skyline.ms>). MS spectra were acquired in the Orbitrap analyzer with a mass range of 300–1750 m/z at
557 a resolution of 70,000 FWHM and a target value of 3×10^6 ions, followed by MS/MS acquisition for the 16
558 targeted precursors. Precursors were selected with an isolation window of 2.0 m/z. HCD fragmentation was
559 performed at a normalized collision energy of 27. MS/MS spectra were acquired with a target value of 2×10^5
560 ions at a resolution of 17,500 FWHM, a maximum injection time of 120 ms and a fixed first mass of m/z 100.

561 **MS data analysis.** Raw data from PRM acquisition were processed using MaxQuant software (version
562 1.5.7.4, <http://www.maxquant.org/>)⁶⁷. MS/MS spectra were searched by the Andromeda search engine
563 against a combined database containing the sequences from *Arabidopsis thaliana* (TAIR10_pep_20101214;
564 ftp://ftp.arabidopsis.org/home/tair/Proteins/TAIR10_protein_lists/) and sequences of 248 common
565 contaminant proteins and decoy sequences. Trypsin specificity was required and a maximum of two missed
566 cleavages allowed. Minimal peptide length was set to seven amino acids. Carbamidomethylation of cysteine
567 residues was set as fixed, phosphorylation of serine, threonine and tyrosine, oxidation of methionine and
568 protein N-terminal acetylation as variable modifications. The match between runs option was disabled.
569 Peptide-spectrum-matches and proteins were retained if they were below a false discovery rate of 1 % in
570 both cases. The “msms.txt” output from MaxQuant was further analyzed using Skyline in PRM mode.
571 Trypsin specificity was required and a maximum of two missed cleavages allowed. Minimal and maximum
572 peptide lengths were set to 7 and 25 amino acids, respectively. Carbamidomethylation of cysteine,

573 phosphorylation of serine, threonine and tyrosine, oxidation of methionine, and protein N-terminal
574 acetylation were set as modifications. Results were filtered for precursor charges of 2 and 3, and b- and y-
575 ions with ion charges of +1 and +2. Product ions were set to “from ion 1 to last ion”. All chromatograms
576 were inspected manually and peak integration was corrected for best representation of MS2 signals. Peak
577 area data was exported and further processed. The Skyline documents containing the data for the targeted
578 phosphoproteomics experiments have been uploaded to Panorama Public and can be obtained
579 from <https://panoramaweb.org/RBOHDphosphorylation.url>. Raw data have been deposited to the
580 ProteomeXchange Consortium via the Panorama partner repository with the dataset identifier PXD013525
581 (<http://proteomecentral.proteomexchange.org/cgi/GetDataset?ID=PX013525>).

582 **Phylogenetic analysis**

583 Sequences for plant *RBOH* genes were extracted from public genome databases and manually curated. The
584 phylogenetic maximum likelihood tree was inferred from a PAGAN⁶⁸ alignment using FASTTREE⁶⁹, 1000
585 bootstrap replicates were calculated using RAxML⁷⁰. The sequence alignment of plant RBOHs, human
586 NOX2 and NOX5 β can be viewed on the Wasabi⁶⁸ webserver (<http://was.bi?id=JauZ6q>). Sequence motifs
587 were analyzed using the MEME suite⁷¹.

588 **Statistical analysis**

589 Statistical analyses were performed with JMP Pro13 (SAS, <https://www.jmp.com/>).

590 **Author contributions**

591 SK, KH, HN and MW conceived and designed the project. SK, KH, LV, CT, AV, AR, LM, MWi, MT, and
592 MWr carried out experiments. SK, KH, LV, AV, AR, TH, MT, and MWr analyzed the data. AH, SCS and
593 HN designed and performed targeted MS analysis and analyzed the data. SK and MWr wrote the manuscript.
594 All authors read and contributed to the final manuscript.

595 **Acknowledgments**

596 The authors would like to thank Dr. Julia Krasensky-Wrzaczek and Dr. Alexey Shapiguzov (University of
597 Helsinki, Finland) for critical comments on the manuscript. We thank Tuomas Puukko, Nghia Le Tri, Simon
598 Schmitz, Denis Owczarek, Jan-Niklas Weber (University of Helsinki, Finland) and Jiaqi Wang (Saitama
599 University, Japan) for technical assistance, Dr. Riccardo Siligato for the Gateway Multisite vector system.
600 We thank Dr. Yasuhiro Kadota (RIKEN Yokohama, Japan) and Prof. Cyril Zipfel (University of Zurich,
601 Switzerland) for *35S::FLAG-RBOHD/rbohD* seeds and pOPINM-RBOHD/N and pBin19g-
602 pRBOHD::3FLAG-RBOHD plasmids. The pcDNA3.1-3FLAG-RBOHD and pcDNA3.1-3FLAG-MCS
603 plasmids were provided by Prof. Kazuyuki Kuchitsu (Tokyo University of Science, Japan). Microscopy
604 imaging was performed at the Light Microscopy Unit, Institute of Biotechnology, University of Helsinki.
605 Mass spectrometry analyses were performed at the Turku Proteomics Facility, supported by Biocenter
606 Finland. LV and TH thank Trude Johansen for technical assistance in LC-MS/MS based hormone analysis.
607 This work was supported by the Academy of Finland (grant numbers #275632, #283139, and #312498 to
608 MW), the University of Helsinki (Three-year fund allocation to MW), the Finnish Cultural Foundation (grant
609 numbers 00170046 and 00181379 to LV), and KAKENHI (17H05007, 18H04775, and 18H05491 to MT),
610 the Max-Planck-Gesellschaft (to HN). KH, SK and MW are members of the Centre of Excellence in the
611 Molecular Biology of Primary Producers (2014-2019) funded by the Academy of Finland (grant numbers
612 #271832 and #307335).

613 **References**

- 614 1. Kimura, S., Waszczak, C., Hunter, K. & Wrzaczek, M. Bound by fate: The role of reactive oxygen
615 species in receptor-like kinase signaling. *Plant Cell* **29**, 638-654 (2017).
- 616 2. Waszczak, C., Carmody, M. & Kangasjärvi, J. Reactive oxygen species in plant signaling. *Annu Rev*
617 *Plant Biol* **69**, 209-236 (2018).
- 618 3. Suzuki, N. *et al.* Respiratory burst oxidases: the engines of ROS signaling. *Curr Opin Plant Biol* **14**,
619 691-699 (2011).
- 620 4. Meitzler, J.L. *et al.* NADPH oxidases: a perspective on reactive oxygen species production in tumor
621 biology. *Antioxid Redox Signal* **20**, 2873-2889 (2014).
- 622 5. Jiménez-Quesada, M.J., Traverso, J.A. & Alché Jde, D. NADPH oxidase-dependent superoxide
623 production in plant reproductive tissues. *Front Plant Sci* **7**, 359 (2016).
- 624 6. Torres, M.A., Dangl, J.L. & Jones, J.D. Arabidopsis gp91^{phox} homologues *AtrbohD* and *AtrbohF* are
625 required for accumulation of reactive oxygen intermediates in the plant defense response. *Proc Natl*
626 *Acad Sci USA* **99**, 517-522 (2002).
- 627 7. Lee, Y., Rubio, M.C., Alassimone, J. & Geldner, N. A mechanism for localized lignin deposition in
628 the endodermis. *Cell* **153**, 402-412 (2013).
- 629 8. Lee, Y. *et al.* A lignin molecular brace controls precision processing of cell walls critical for surface
630 integrity in *Arabidopsis*. *Cell* **173**, 1468-1480 (2018).

- 631 9. Kaya, H. *et al.* Comparative analysis of the reactive oxygen species-producing enzymatic activity of
632 Arabidopsis NADPH oxidases. *Plant J* (2018).
- 633 10. Zhang, M. *et al.* The MAP4 kinase SIK1 ensures robust extracellular ROS burst and antibacterial
634 immunity in plants. *Cell Host Microbe* **24**, 379-391 (2018).
- 635 11. Kadota, Y. *et al.* Direct regulation of the NADPH oxidase RBOHD by the PRR-associated kinase
636 BIK1 during plant immunity. *Mol Cell* **54**, 43-55 (2014).
- 637 12. Li, L. *et al.* The FLS2-associated kinase BIK1 directly phosphorylates the NADPH oxidase RbohD
638 to control plant immunity. *Cell Host Microbe* **15**, 329-338 (2014).
- 639 13. Dubiella, U. *et al.* Calcium-dependent protein kinase/NADPH oxidase activation circuit is required
640 for rapid defense signal propagation. *Proc Natl Acad Sci USA* **110**, 8744-8749 (2013).
- 641 14. Han, J.P. *et al.* Fine-tuning of RBOHF activity is achieved by differential phosphorylation and Ca²⁺
642 binding. *New Phytol* **221**, 1935-1949 (2019).
- 643 15. Kimura, S. *et al.* Protein phosphorylation is a prerequisite for the Ca²⁺-dependent activation of
644 Arabidopsis NADPH oxidases and may function as a trigger for the positive feedback regulation of
645 Ca²⁺ and reactive oxygen species. *Biochim Biophys Acta* **1823**, 398-405 (2012).
- 646 16. Ogasawara, Y. *et al.* Synergistic activation of the Arabidopsis NADPH oxidase AtrbohD by Ca²⁺ and
647 phosphorylation. *J Biol Chem* **283**, 8885-8892 (2008).
- 648 17. Raad, H. *et al.* Regulation of the phagocyte NADPH oxidase activity: phosphorylation of
649 gp91^{phox}/NOX2 by protein kinase C enhances its diaphorase activity and binding to Rac2, p67^{phox},
650 and p47^{phox}. *FASEB J* **23**, 1011-1022 (2009).
- 651 18. Jagnandan, D. *et al.* Novel mechanism of activation of NADPH oxidase 5. Calcium sensitization via
652 phosphorylation. *J Biol Chem* **282**, 6494-6507 (2007).
- 653 19. Shiu, S.H. & Bleecker, A.B. Receptor-like kinases from Arabidopsis form a monophyletic gene
654 family related to animal receptor kinases. *Proc Natl Acad Sci USA* **98**, 10763-10768 (2001).
- 655 20. Couto, D. & Zipfel, C. Regulation of pattern recognition receptor signalling in plants. *Nat Rev*
656 *Immunol* **16**, 537-552 (2016).
- 657 21. Vaattovaara, A. *et al.* Mechanistic insights into the evolution of DUF26-containing proteins in land
658 plants. *Commun Biol* **2**, 56 (2019).
- 659 22. Idänheimo, N. *et al.* The Arabidopsis thaliana cysteine-rich receptor-like kinases CRK6 and CRK7
660 protect against apoplastic oxidative stress. *Biochem Biophys Res Commun* **445**, 457-462 (2014).
- 661 23. Yeh, Y.H., Chang, Y.H., Huang, P.Y., Huang, J.B. & Zimmerli, L. Enhanced Arabidopsis pattern-
662 triggered immunity by overexpression of cysteine-rich receptor-like kinases. *Front Plant Sci* **6**, 322
663 (2015).
- 664 24. Yadeta, K.A. *et al.* A cysteine-rich protein kinase associates with a membrane immune complex and
665 the cysteine residues are required for cell death. *Plant Physiol* **173**, 771-787 (2017).
- 666 25. Bourdais, G. *et al.* Large-scale phenomics identifies primary and fine-tuning roles for CRKs in
667 responses related to oxidative stress. *PLOS Genetics* **11**, e1005373 (2015).
- 668 26. Chen, K., Fan, B., Du, L. & Chen, Z. Activation of hypersensitive cell death by pathogen-induced
669 receptor-like protein kinases from Arabidopsis. *Plant Mol Biol* **56**, 271-283 (2004).
- 670 27. Wrzaczek, M. *et al.* Transcriptional regulation of the CRK/DUF26 group of receptor-like protein
671 kinases by ozone and plant hormones in Arabidopsis. *BMC Plant Biol* **10**, 95 (2010).
- 672 28. Acharya, B.R. *et al.* Overexpression of CRK13, an Arabidopsis cysteine-rich receptor-like kinase,
673 results in enhanced resistance to *Pseudomonas syringae*. *Plant J* **50**, 488-499 (2007).
- 674 29. Chern, M. *et al.* A genetic screen identifies a requirement for cysteine-rich-receptor-like kinases in
675 rice NH1 (OsNPR1)-mediated immunity. *PLoS Genet* **12**, e1006049 (2016).
- 676 30. Tanaka, H. *et al.* Abiotic stress-inducible receptor-like kinases negatively control ABA signaling in
677 Arabidopsis. *Plant J* **70**, 599-613 (2012).
- 678 31. Hunter, K. *et al.* CRK2 enhances salt tolerance by regulating callose deposition in connection with
679 PLDα1. *bioRxiv*, 487009 (2019).
- 680 32. Stone, J.M. & Walker, J.C. Plant protein kinase families and signal transduction. *Plant Physiol* **108**,
681 451-457 (1995).
- 682 33. Horikawa, K. *et al.* Spontaneous network activity visualized by ultrasensitive Ca²⁺ indicators, yellow
683 Cameleon-Nano. *Nat Methods* **7**, 729-732 (2010).
- 684 34. Benschop, J.J. *et al.* Quantitative phosphoproteomics of early elicitor signaling in Arabidopsis. *Mol*
685 *Cell Proteomics* **6**, 1198-1214 (2007).

- 686 35. Kadota, Y., Shirasu, K. & Zipfel, C. Regulation of the NADPH Oxidase RBOHD During Plant
687 Immunity. *Plant Cell Physiol* **56**, 1472-80 (2015).
- 688 36. Schmidt, R., Kunkowska, A.B. & Schippers, J.H. Role of reactive oxygen species during cell
689 expansion in leaves. *Plant Physiol* **172**, 2098-2106 (2016).
- 690 37. Ellinger, D. & Voigt, C.A. Callose biosynthesis in Arabidopsis with a focus on pathogen response:
691 what we have learned within the last decade. *Ann Bot* **114**, 1349-1358 (2014).
- 692 38. Caillaud, M.C. *et al.* The plasmodesmal protein PDL1 localises to haustoria-associated membranes
693 during downy mildew infection and regulates callose deposition. *PLoS Pathog* **10**, e1004496 (2014).
- 694 39. Boudsocq, M., Danquah, A., de Zelicourt, A., Hirt, H. & Colcombet, J. Plant MAPK cascades: Just
695 rapid signaling modules? *Plant Signal Behav* **10**, e1062197 (2015).
- 696 40. Bigeard, J., Colcombet, J. & Hirt, H. Signaling mechanisms in pattern-triggered immunity (PTI).
697 *Mol Plant* **8**, 521-539 (2015).
- 698 41. Beaumel, S. *et al.* Down-regulation of NOX2 activity in phagocytes mediated by ATM-kinase
699 dependent phosphorylation. *Free Radic Biol Med* **113**, 1-15 (2017).
- 700 42. Banfi, B. *et al.* Mechanism of Ca²⁺ activation of the NADPH oxidase 5 (NOX5). *J Biol Chem* **279**,
701 18583-18591 (2004).
- 702 43. Pandey, D., Gratton, J.P., Rafikov, R., Black, S.M. & Fulton, D.J. Calcium/calmodulin-dependent
703 kinase II mediates the phosphorylation and activation of NADPH oxidase 5. *Mol Pharmacol* **80**,
704 407-415 (2011).
- 705 44. Chen, F. *et al.* Regulation of NADPH oxidase 5 by protein kinase C isoforms. *PLoS One* **9**, e88405
706 (2014).
- 707 45. Yun, B.W. *et al.* S-nitrosylation of NADPH oxidase regulates cell death in plant immunity. *Nature*
708 **478**, 264-268 (2011).
- 709 46. Lin, Z.J., Liebrand, T.W., Yadeta, K.A. & Coaker, G. PBL13 Is a serine/threonine protein kinase
710 that negatively regulates Arabidopsis immune responses. *Plant Physiol* **169**, 2950-2962 (2015).
- 711 47. Chen, D. *et al.* Extracellular ATP elicits DORN1-mediated RBOHD phosphorylation to regulate
712 stomatal aperture. *Nat Commun* **8**, 2265 (2017).
- 713 48. Zhang, J. *et al.* Receptor-like cytoplasmic kinases integrate signaling from multiple plant immune
714 receptors and are targeted by a *Pseudomonas syringae* effector. *Cell Host Microbe* **7**, 290-301
715 (2010).
- 716 49. Lee, D.S.K., Young Cheon; Kwon, Sun Jae; Ryu, Choong-Min; Park, Ohkmae K. The Arabidopsis
717 cysteine-rich receptor-like kinase CRK36 regulates immunity through interaction with the
718 cytoplasmic kinase BIK1. *Frontiers in Plant Science* **8**, 1856 (2017).
- 719 50. Kaya, H. *et al.* Ca²⁺-activated reactive oxygen species production by Arabidopsis RbohH and RbohJ
720 is essential for proper pollen tube tip growth. *Plant Cell* **26**, 1069-1080 (2014).
- 721 51. Zipfel, C. *et al.* Bacterial disease resistance in Arabidopsis through flagellin perception. *Nature* **428**,
722 764-767 (2004).
- 723 52. Veronese, P. *et al.* The membrane-anchored BOTRYTIS-INDUCED KINASE1 plays distinct roles in
724 Arabidopsis resistance to necrotrophic and biotrophic pathogens. *Plant Cell* **18**, 257-273 (2006).
- 725 53. Denness, L. *et al.* Cell wall damage-induced lignin biosynthesis is regulated by a reactive oxygen
726 species- and jasmonic acid-dependent process in Arabidopsis. *Plant Physiol* **156**, 1364-1374 (2011).
- 727 54. Clough, S.J. & Bent, A.F. Floral dip: a simplified method for *Agrobacterium*-mediated
728 transformation of *Arabidopsis thaliana*. *Plant J* **16**, 735-743 (1998).
- 729 55. Siligato, R. *et al.* MultiSite gateway-compatible cell type-specific gene-inducible system for plants.
730 *Plant Physiol* **170**, 627-641 (2016).
- 731 56. Gookin, T.E. & Assmann, S.M. Significant reduction of BiFC non-specific assembly facilitates in
732 planta assessment of heterotrimeric G-protein interactors. *Plant J* **80**, 553-567 (2014).
- 733 57. Sierla, M. *et al.* The receptor-like pseudokinase GHR1 is required for stomatal closure. *Plant Cell* **30**,
734 2813-2837 (2018).
- 735 58. Kawarazaki, T. *et al.* A low temperature-inducible protein AtSRC2 enhances the ROS-producing
736 activity of NADPH oxidase AtRbohF. *Biochim Biophys Acta* **1833**, 2775-2780 (2013).
- 737 59. Whalen, M.C., Innes, R.W., Bent, A.F. & Staskawicz, B.J. Identification of *Pseudomonas syringae*
738 pathogens of Arabidopsis and a bacterial locus determining avirulence on both Arabidopsis and
739 soybean. *Plant Cell* **3**, 49-59 (1991).

- 740 60. Wrzaczek, M., Rozhon, W. & Jonak, C. A Proteasome-regulated glycogen synthase kinase-3
741 modulates disease response in plants. *J Biol Chem* **282**, 5249-5255 (2007).
- 742 61. Forcat, S., Bennett, M.H., Mansfield, J.W. & Grant, M.R. A rapid and robust method for
743 simultaneously measuring changes in the phytohormones ABA, JA and SA in plants following biotic
744 and abiotic stress. *Plant Methods* **4**, 16 (2008).
- 745 62. Kadota, Y., Macho, A.P. & Zipfel, C. Immunoprecipitation of plasma membrane receptor-like
746 kinases for identification of phosphorylation sites and associated proteins. *Methods Mol Biol* **1363**,
747 133-144 (2016).
- 748 63. Fujiwara, T., Hirai, M.Y., Chino, M., Komeda, Y. & Naito, S. Effects of sulfur nutrition on
749 expression of the soybean seed storage protein genes in transgenic petunia. *Plant Physiol* **99**, 263-
750 268 (1992).
- 751 64. Sugiyama, N. *et al.* Phosphopeptide enrichment by aliphatic hydroxy acid-modified metal oxide
752 chromatography for nano-LC-MS/MS in proteomics applications. *Mol Cell Proteomics* **6**, 1103-1109
753 (2007).
- 754 65. Nakagami, H. StageTip-based HAMMOC, an efficient and inexpensive phosphopeptide enrichment
755 method for plant shotgun phosphoproteomics. *Methods Mol Biol* **1072**, 595-607 (2014).
- 756 66. MacLean, B. *et al.* Skyline: an open source document editor for creating and analyzing targeted
757 proteomics experiments. *Bioinformatics* **26**, 966-968 (2010).
- 758 67. Cox, J. & Mann, M. MaxQuant enables high peptide identification rates, individualized p.p.b.-range
759 mass accuracies and proteome-wide protein quantification. *Nat Biotechnol* **26**, 1367-1372 (2008).
- 760 68. Löytynoja A, Vilella AJ, Goldman N. Accurate extension of multiple sequence alignments using a
761 phylogeny-aware graph algorithm. *Bioinformatics* **28**:1684-91 (2012).
- 762 69. Price, M.N., Dehal, P.S. & Arkin, A.P. FastTree 2--approximately maximum-likelihood trees for
763 large alignments. *PLoS One* **5**, e9490 (2010).
- 764 70. Stamatakis, A. RAxML version 8: a tool for phylogenetic analysis and post-analysis of large
765 phylogenies. *Bioinformatics* **30**, 1312-1313 (2014).
- 766 71. Bailey, T.L. *et al.* MEME SUITE: tools for motif discovery and searching. *Nucleic Acids Res* **37**,
767 W202-8 (2009).

768

769

770 **Figure legends:**

771 **Fig. 1 CRK2 kinase activity is required for plant growth.**

772 **a** Schematic representation of CRK2 structure. SP: signal peptide (AAs 1-29), DUF26-A (AAs 39-132),
773 DUF26-B (AAs 146-243), TM: transmembrane domain (AAs 261-283), and kinase domain (AAs 325-601).

774 **b** Representative pictures of 21-day-old plants of Col-0, *crk2*, *CRK2pro::CRK2-YFP/crk2*,
775 *CRK2pro::CRK2^{K353E}-YFP/crk2* and *CRK2pro::CRK2^{D450N}-YFP/crk2* plants. Bar = 1 cm.

776 **c** Box plot shows the fresh weight of 21-day-old plants (n = 10). Differences between Col-0 and transgenic
777 lines were evaluated with One-way Anova with Tukey-Kramer HSD, *** p<0.001, ns, not statistically
778 significant (Oneway Anova, F value = 71.5559, DF = 7). The experiment was repeated three times with
779 similar results.

780 **d** Subcellular localization of CRK2-YFP, CRK2^{K353E}-YFP and CRK2^{D450N}-YFP in leaves of 7-day-old
781 seedlings. Plasma membrane localization was confirmed using plasmolysis to visualize Hechtian strands
782 (arrow heads). Plasmolysis was induced by the application of 0.8 M mannitol. Scale bar = 25 μ m.

783

784 **Fig. 2 CRK2 regulates flg22-triggered immunity and resistance to a virulent bacterial pathogen.**

785 **a** and **b** flg22-induced ROS production in Col-0, *crk2* and *CRK2pro::CRK2-YFP/crk2* or
786 *CRK2pro::CRK2^{D450N}-YFP/crk2*. Leaf discs from 28-day-old plants were treated with 200 nM flg22 and
787 ROS production was measured. Box plot shows cumulative ROS production over 40 min (upper right).

788 **a** Values represent mean \pm SEM of n \geq 16. Differences compared with Col-0 were evaluated with One-way
789 Anova (F value = 9.2282, DF = 3) with Tukey-Kramer HSD, *** p < 0.001, ns, not statistically significant.

790 **b** Values represent the mean \pm SEM of n \geq 19. Differences compared with Col-0 were evaluated with One-
791 way Anova (F value = 8.8777, DF = 3) with Tukey-Kramer HSD, *p < 0.05, *** p < 0.001.

792 **c** Quantitative analysis of bacterial growth in Col-0, *crk2* and *CRK2pro::CRK2-YFP/crk2* or
793 *CRK2pro::CRK2^{D450N}-YFP/crk2* following syringe infiltration with *Pto* DC3000 (1 x 10⁵ CFU/mL). Values
794 represent mean \pm SD of n = 3 (0 DPI) or n = 6 (2 DPI). Letters indicate significant differences at p < 0.05
795 [One-way Anova (F value = 566.5661, DF = 11) with Tukey-Kramer HSD].

796 **d** Quantitative analysis of cytosolic Ca²⁺ changes in response to 10 μ M flg22 in 7-day-old *YCNano65* or
797 *YCNano65/crk2* seedlings. Values represent the mean \pm SEM of n = 9 (*YCNano65*) or n = 15
798 (*YCNano65/crk2*).

799 **e** Representative frame images of cytosolic Ca²⁺ change in wild type and *crk2* plants. Bar = 0.5 mm.

800 **a - e** The experiment was repeated three times with similar results.

801

802 **Fig. 3 CRK2 interacts with RBOHD.**

803 **a** ROS production of RBOHD-expressing HEK293T cells. 3FLAG-RBOHD was transiently co-expressed
804 with either 3Myc-GFP or CRK2 (WT or D450N)-3Myc. After 30 min 1 μ M ionomycin was added to the
805 medium. Values represent mean \pm SEM of n = 3. E.V. = empty vector. The experiment was repeated three
806 times with similar results.

807 **b** and **c** Co-IP analysis of interaction between RBOHD and CRK2. CRK2-YFP was immuno-precipitated
808 using anti-GFP beads followed by immunoblotting with anti-RBOHD and anti-GFP antibodies. FLAG-
809 RBOHD: 105 kDa, CRK2-YFP: 99.9 kDa and YFP-6Myc: 36.7 kDa.

810 **b** *35S::FLAG-RBOHD/rbohD x 35S::CRK2-YFP/Col-0* (F1) and *35S::FLAG-RBOHD/rbohD x 35S::YFP-*
811 *6Myc/Col-0* (F1) plants. The experiment was repeated three times with similar results.

812 **c** *35S::FLAG-RBOHD/35S::CRK2-YFP/rbohD* plants with 1 μ M flg22 treatment. M: Protein molecular
813 marker, *: unspecific signal. Total protein from *rbohD* was used for immunoblot of input as a negative
814 control.

815 **d** Schematic representation of RBOHD structure. EF-hands (AAs 257-329), TM: transmembrane domains
816 (AAs 374 - 605), FAD: FAD-binding domain (AAs 613-730), NADPH: NADPH-binding domain (AAs 736-
817 904), RBOHD/N: RBOHD N-terminal region (AAs 1-376), RBOHD/C: RBOHD C-terminal region (AAs
818 606-922); C1: RBOHD/C1 (AAs 606-741), C2: RBOHD/C2 (AAs 696-831), C3: RBOHD/C3 (AAs 787-
819 922).

820 **e** *In vitro* pull-down analysis of direct interaction between RBOHD and CRK2. MBP, 6His-MBP-RBOHD/N
821 and 6His-MBP-RBOHD/C were incubated with 6His-GST-CRK2cyto and pull down with GST followed by
822 immunoblotting with anti-6His and anti-MBP antibodies. 6His-GST-CRK2cyto: 68.5 kDa, 6His-MBP-
823 RBOHD/N: 84.7 kDa, 6His-MBP-RBOHD/C: 78.4 kDa, MBP: 50.8 kDa. The experiment was repeated two
824 times with similar results.

825

826 **Fig. 4 CRK2 phosphorylates the cytosolic regions of RBOHD in vitro.**

827 **a** and **b** Autophosphorylation and transphosphorylation were visualized with [γ -³²P] ATP and
828 autoradiography (upper panel). Input proteins were stained with coomassie brilliant blue (CBB) (lower
829 panel). Experiments were repeated three times with similar results. 6His-GST-CRK2cyto: 68.5 kDa, 6His-
830 MBP-RBOHD/N: 84.7 kDa, 6His-MBP-RBOHD/C1:57.9 kDa, /C2:57.8 kDa, /C3:58.4 kDa, 6His-MBP:
831 44.3 kDa.

832 **a** *In vitro* transphosphorylation of 6His-MBP-RBOHD N-terminus by 6His-GST-CRK2cyto. 6His-MBP-
833 RBOHD/N or 6His-MBP was incubated with 6His-GST-CRK2cyto in kinase buffer.

834 **b** *In vitro* transphosphorylation of 6His-MBP-RBOHD C-terminus by 6His-GST-CRK2cyto. 6His-MBP-
835 RBOHD/C1, /C2, /C3 or 6His-MBP was incubated with 6His-GST-CRK2cyto in kinase buffer.

836

837 **Fig. 5 CRK2 modulates the ROS-production activity of RBOHD via phosphorylation of the C-**
838 **terminus in HEK293T cells.**

839 **a** Effect of mutations of CRK2-dependent *in vitro* phosphorylation sites in the N-terminal cytosolic region of
840 RBOHD. 3FLAG-RBOHD (WT, S8A or S39A) was transiently co-expressed with either 3Myc-GFP or
841 CRK2-3Myc in HEK293T cells. After 30 min 1 μ M ionomycin was added to the medium to promote Ca^{2+}
842 influx. Values represent mean \pm SEM of n = 3. E.V. = empty vector. The experiment was repeated three times
843 with similar results.

844 **b** Effect of mutations in the CRK2-dependent *in vitro* phosphorylation sites in the C-terminal cytosolic
845 region of RBOHD. 3FLAG-RBOHD (WT, S611A, S703A or S862A) were transiently co-expressed with
846 either 3Myc-GFP or CRK2-3Myc in HEK293T cells. After 30 min 1 μ M ionomycin was added to the
847 medium to promote Ca^{2+} influx. Values represent mean \pm SEM of n = 3. E.V. = empty vector. The
848 experiment was repeated three times with similar results.

849

850 **Fig. 6 RBOHD S703 and S862 are involved in regulation of flg22-induced ROS production.**

851 **a - c** Quantification of RBOHD phosphorylation in Col-0 upon flg22 treatment. 12-day-old seedlings were
852 treated with water (-) or 1 μ M flg22 (+) for 5 min. Total proteins were digested with trypsin (S8 and S39) or
853 Lys-C (S703) and phosphopeptides were enriched, and then selected phosphopeptides were quantified by
854 LC-MS/MS. Box plots show MS2 fragment peak ion areas of indicated phosphopeptides (n = 4). Differences
855 between water- or flg22-treated samples were evaluated with One-way Anova (DF = 1) with Tukey-Kramer
856 HSD, *** p<0.001, ns, not statistically significant.

857 **a** RBOHD S8 residue (F value = 0.4745).

858 **b** RBOHD S39 residue (F value = 51.3297).

859 **c** RBOHD S703 residue (F value = 41.0851).

860 **d** and **e** flg22-induced ROS production. Leaf discs from 28-day-old plants were treated with 200 nM flg22.
861 Box plot shows cumulative ROS production over 40 min (upper right). The experiment was repeated three
862 times with similar results.

863 **d** flg22-induced ROS production in *RBOHDpro::3FLAG-RBOHD/rbohD* #1-3 and *RBOHDpro::3FLAG-*
864 *RBOHD^{S703A}/rbohD* #3-2. Values represent mean \pm SEM of n \geq 23. Difference between lines was evaluated
865 with One-way Anova (F value = 4.4509, DF = 1) with Tukey-Kramer HSD, * p < 0.05.

866 e flg22-induced ROS production in *RBOHDpro::3FLAG-RBOHD/rbohD* #11-3 and *RBOHDpro::3FLAG-*
867 *RBOHD^{S862A}/rbohD* #1-6. Values represent mean \pm SEM of n = 24. Difference between lines was evaluated
868 with One-way Anova (F value = 8.5305, DF = 1) with Tukey-Kramer HSD, ** p < 0.01.

869

870 **Fig. 7 Phosphorylation sites in the C-terminal region are conserved in plants and animals.**

871 Phylogenetic tree showing that plant RBOHs form a single clade which is parallel to the NADPH oxidases
872 NOX2 and NOX5 β from *Homo sapiens*. The sequence context of the phospho-site S8 in RBOHD is only
873 conserved RBOHD from *Arabidopsis thaliana* and *Capsella rubella*. The tree was constructed using
874 FASTTREE from a PAGAN alignment in WASABI, 1000 bootstraps were calculated with RAxML. The full
875 sequence alignment can be found in Wasabi at <http://was.bi?id=JauZ6q>. Plant species included were:
876 *Arabidopsis thaliana* (At), *Capsella rubella* (Cr), *Prunus persica* (Pp), *Solanum lycopersicum* (Sl), *Aquilegia*
877 *coerulea* (Ac), *Oryza sativa* (Os), *Sorghum bicolor* (Sb), *Amborella trichopoda* (Atr), and *Marchantia*
878 *polymorpha* (Mp). Numbers of phospho-sites in the meme figures represent the position of the amino acid in
879 RBOHD from *Arabdiopsis thaliana*. Arrows indicate the position of the phospho-site (S or T) or
880 corresponding amino acid.

881

882 **Fig. 8 Schematic model for MAMP-triggered RBOHD activation.**

883 MAMPs are recognized by MAMP receptor complexes. RBOHD N-terminus is phosphorylated by BIK1 and
884 SIK1 and apoplastic ROS production is induced. Apoplastic ROS production by RBOHD leads to Ca²⁺
885 influx into the cytosol. Ca²⁺-binding to RBOHD N-terminus and to CPKs leads to Ca²⁺-dependent activation
886 of RBOHD. We found that CRK2 also contributes to the activation of RBOHD *via* phosphorylation of its C-
887 terminus at S703. CRK2 can also mediate inhibition of MAPK activation and callose deposition *via* CALS
888 after MAMP perception. MPK, mitogen-activated protein kinase; MP2K, MPKK; MP3K, MPKKK.

889

890 **Supplementary figure legends**

891 **Fig. S1 Complementation of *crk2* with *CRK2pro::CRK2-YFP*.**

892 **a** Box plot shows dry weight of 21-day-old plants (n = 10). Differences compared with Col-0 were evaluated
893 with One-way Anova with Tukey-Kramer HSD, *** p < 0.001, ns, not statistically significant (One-way
894 Anova, F value = 48.2539, DF = 7). The experiment was repeated three times with similar results.

895 **b** Salicylic acid accumulation level in Col-0, *crk2* and *CRK2pro::CRK2-YFP/crk2* #1-22. 6-day-old
896 seedlings were used. Differences compared with Col-0 were evaluated with One-way Anova (F value =
897 3.0476, DF = 2) with Tukey-Kramer HSD. ns, not statistically significant.

898 **c** *In vitro* transphosphorylation of MyBP (Myelin Basic Protein) by 6His-GST-CRK2cyto. Artificial
899 substrate MyBP was incubated without or with 6His-GST-CRK2cyto WT or kinase-dead (KD: K353E or
900 D450N) in kinase buffer. Autophosphorylation and transphosphorylation were visualized with [γ -³²P] ATP
901 and autoradiography (upper panel). Proteins stained with coomassie brilliant blue (CBB) staining (lower
902 panel). Molecular weights of recombinant proteins: 6His-GST-CRK2cyto: 68.5 kDa, MyBP: 18.4 kDa. The
903 experiment was repeated three times with similar results.

904 **d** Subcellular localization of CRK2-YFP, CRK2^{K353E}-YFP and CRK2^{D450N}-YFP in leaves of 7-day-old
905 seedlings. Plasma membrane localization was confirmed using plasmolysis to visualize Hechtian strands
906 (arrow head). Plasmolysis was induced by the application of 0.8 M mannitol. Scale bar = 25 μ m.

907

908 **Fig. S2 MAMP-triggered ROS production and molecular responses in *crk2*.**

909 **a** and **b** Box plot shows quantitative real-time RT-PCR (qPCR) analysis of *FRKI* (a) or *NHL10* (b)
910 transcripts in Col-0, *crk2* and *fls2* after treatment with flg22 (n = 3, biological replicates). 10-day-old plants
911 were incubated in 1 μ M flg22 solution and collected at indicated time (each time point contains 90 plants per
912 genotype). Transcript levels were calculated by comparison with non-treated Col-0 (Time = 0).

913 **a** *FRKI* expression. Different letters indicate significant difference at p < 0.05 [One-way Anova (F value =
914 9.4471, DF = 11) with Tukey-Kramer HSD].

915 **b** *NHL10* expression. Different letters indicate significant difference at p < 0.05 [One-way Anova (F value =
916 9.1059, DF = 11) with Tukey-Kramer HSD].

917 **c** and **d** Chitin- or AtPep1- induced ROS production in Col-0, *crk2* and *rbohD*. Leaf discs from 28-day-old
918 plants were treated with 200 μ g/mL chitin (b) or 1 μ M AtPep1 (c). ROS production is expressed in relative
919 luminescence units (RLU). Box plots show integration of ROS production for 40 min (upper right). The
920 experiment was repeated three times with similar results.

921 **c** Values represent the mean \pm SEM of n \geq 21. Differences compared with Col-0 were evaluated with One-
922 way Anova (F value = 24.1435, DF = 2) with Tukey-Kramer HSD, * p < 0.05, *** p < 0.001.

923 **d** Values represent the mean \pm SEM of n = 24. Differences compared with Col-0 were evaluated with One-
924 way Anova (F value = 44.5132, DF = 2) with Tukey-Kramer HSD, *** p < 0.001.

925 **e** MAPK activation in Col-0, *crk2* and *fls2* in response to treatment with 1 μ M flg22. 28-day-old plants (12
926 plants per genotype). Phosphorylated MPK3 and MPK6 were detected with anti-p44/42 MPK antibody
927 (upper panel). Proteins stained with amido black staining (lower panel). The experiment was repeated three
928 times with similar results.

929 **f** Quantification of flg22-induced callose deposition by aniline blue ($n \geq 16$) in 7-day-old seedlings with (+)
930 or without (-) treatment with 10 μM flg22 for 30 min. Letters indicate significant differences at $p < 0.05$
931 [One-way Anova (F value = 44.8732, DF = 3) with Tukey-Kramer HSD].

932 **g** Representative images of aniline blue stained leaves. Bar = 100 μm .

933

934 **Fig. S3 CRK2 modulates the ROS-producing activity of RBOHC, D and F in HEK293T cells.**

935 **a** Expressed proteins were detected by anti-FLAG and anti-Myc antibodies (Fig. 3a). 3FLAG-RBOHD: 107
936 kDa, CRK2-3Myc: 75.8 kDa, 3Myc-GFP: 31 kDa, β -actin 42 kDa. As a loading control, β -actin was used.
937 Loading volume for anti-Myc antibody: 3FLAG-RBOHD + 3Myc-GFP (5 μL), the others (50 μL).

938 **b** ROS production in RBOHD-expressing HEK293T cells in Ca^{2+} -free buffer. 3FLAG-RBOHD was
939 transiently co-expressed with either 3Myc-GFP or 3Myc-CRK2 (WT or D450N) in HEK293T cells. Values
940 represent mean \pm SEM of $n = 3$. E.V. = empty vector. The experiment was repeated three times with similar
941 results.

942 **c** Proteins expressed in HEK293T cells were detected by anti-FLAG and anti-Myc antibodies (Fig. S3b).
943 3FLAG-RBOHD: 107 kDa, CRK2-3Myc: 75.8 kDa, 3Myc-GFP: 31 kDa, β -actin 42 kDa. As a loading
944 control, β -actin was used. Loading volume for anti-Myc antibody: 3FLAG-RBOHD + 3Myc-GFP (5 μL),
945 others (50 μL).

946 **d - f** ROS production of RBOHD-, RBOHC-, or RBOHF-expressing HEK293T cells. 3FLAG-RBOHD (**d**),
947 3FLAG-RBOHC (**e**), or 3FLAG-RBOHF (**f**) was transiently co-expressed with 3Myc-GFP or CRK2-3Myc
948 in HEK293T cells, respectively. After 20 min of base line measurement, 1 μM ionomycin was added to the
949 medium. Values represent mean \pm SEM of $n = 3$. The experiment was repeated two times with similar results.

950 **g** Proteins expressed in HEK293T cells were detected by anti-FLAG and anti-Myc antibodies (Fig. S3d-f).
951 3FLAG-RBOHD: 107 kDa, 3FLAG-RBOHC, 106 kDa, 3FLAG-RBOHF: 111 kDa, CRK2-3Myc: 75.8 kDa,
952 3Myc-GFP: 31 kDa, β -actin 42 kDa. As a loading control, β -actin was used. Loading volume for anti-Myc
953 antibody: 3FLAG-RBOHs + 3Myc-GFP (5 μL), 3FLAG-RBOHs + CRK2-3Myc (50 μL).

954 **h** BiFC analysis of interaction between RBOHD and CRK2. The proteins were transiently expressed in
955 *Nicotiana benthamiana* epidermal cells. As a negative control, NmVen210::RBOHD-GUS::Cven210 was
956 used. Merge pictures shows mTq2-Golgi signal marking transformed cells (blue) and autofluorescence (red).
957 Bar = 25 μm .

958

959

960

961 **Fig. S4 BIK1 phosphorylates the N-terminus of RBOHD *in vitro*.**

962 *In vitro* transphosphorylation of 6His-MBP-RBOHD N-terminus by 6His-GST-CRK2cyto and GST-BIK1.
963 6His-MBP-RBOHD/N or 6His-MBP was incubated with 6His-GST-CRK2cyto or GST-BIK1 in kinase
964 buffer. Autophosphorylation and transphosphorylation were visualized with [γ - 32 P] ATP and
965 autoradiography (upper panel). Input proteins were stained with coomassie brilliant blue (CBB) (lower
966 panel). Experiments were repeated three times with similar results. 6His-GST-CRK2cyto: 68.5 kDa, GST-
967 BIK1: 70.9 kDa, 6His-MBP-RBOHD/N: 84.7 kDa, 6His-MBP: 44.3 kDa.

968

969 **Fig. S5 ROS production activity of RBOHD S703A and S862A in HEK293T cells.**

970 **a** and **b** Proteins expressed in HEK293T cells were detected by anti-FLAG and anti-Myc antibodies (Fig. 5a
971 and 5b). 3FLAG-RBOHD: 107 kDa, CRK2-3Myc: 75.8 kDa, 3Myc-GFP: 31 kDa, β -actin 42 kDa. As a
972 loading control, β -actin was used. Loading volume for anti-Myc antibody: 3FLAG-RBOHD + 3Myc-GFP (5
973 μ L), others (50 μ L).

974 **a** 3FLAG-RBOHD (WT, S8A or S39A) was transiently co-expressed with either 3Myc-GFP or CRK2-3Myc
975 into HEK293T cells.

976 **b** 3FLAG-RBOHD (WT, S611A, S703A or S862A) was transiently co-expressed with either 3Myc-GFP or
977 CRK2-3Myc into HEK293T cells.

978 **c** and **d** ROS production of RBOHD-expressing HEK293T cells. After 30 min 1 μ M ionomycin was added to
979 the medium. Values represent mean \pm SEM of n = 3. E.V. = empty vector. The experiment was repeated three
980 times with similar results.

981 **c** 3FLAG-RBOHD (WT or S703A) was transiently co-expressed with either 3Myc-GFP or CRK2-3Myc into
982 HEK293T cells.

983 **d** 3FLAG-RBOHD (WT or S862A) was transiently co-expressed with either 3Myc-GFP or CRK2-3Myc into
984 HEK293T cells.

985

986 **Fig. S6 Quantification of RBOHD and MPK phosphorylation in Col-0 upon flg22 treatment.**

987 12-day-old Col-0 seedlings were treated with water (-) or 1 μ M flg22 (+) for 5 min. Total proteins were
988 digested by trypsin for peptides from RBOHD N-terminal region and MPKs, by Lys-C for RBOHD S703
989 peptide. Peptides were enriched, and then selected phosphopeptides were quantified by LC-MS/MS. Box
990 plots show MS2 fragment peak ion areas of indicated phosphopeptides (n = 4). Differences between water-
991 or flg22-treated samples were evaluated with One-way Anova (DF = 1) with Tukey-Kramer HSD, * P<0.05,
992 ** P<0.01, *** p<0.001, ns, not statistically significant.

993 **a** and **b** RBOHD S8 residue [F value = 9.3550 (a), F value = 1.7274 (b)].

994 **c** RBOHD S39 residue (F value = 51.1741).

995 **d** RBOHD S703 residue (F value = 87.8835).

996 **e** RBOHD S163 residue (F value = 71.8320).

997 **f** RBOHD S347 residue (F value = 22.8032).

998 **g** RBOHD S343 and S347 residues (F value = 10.9184).

999 **h** MPK3 TEY motif (F value = 8.0906).

1000 **i** MPK6 TEY motif (F value = 33.9863).

1001 **j** MPK11 TEY motif (F value = 11.6362).

1002

1003 **Fig. S7 RBOHD S703 and S862 are involved in regulation of flg22-induced ROS production.**

1004 **a** Representative pictures of 21-day-old plants of *RBOHDpro::3FLAG-RBOHD/rbohD*,
1005 *RBOHDpro::3FLAG-RBOHD^{S703A}/rbohD* and *RBOHDpro::3FLAG-RBOHD^{S862A}/rbohD* plants. Bar = 1 cm.

1006 **b** and **c** 3FLAG-RBOHD was detected by anti-FLAG antibody. Input proteins stained with amido black
1007 staining (lower panel).

1008 **b** Expressed proteins in *RBOHDpro::3FLAG-RBOHD/rbohD* #1-3 and *RBOHDpro::3FLAG-*
1009 *RBOHD^{S703A}/rbohD* #3-2.

1010 **c** Expressed proteins in *RBOHDpro::3FLAG-RBOHD/rbohD* #11-3 and *RBOHDpro::3FLAG-*
1011 *RBOHD^{S862A}/rbohD* #1-6.

1012 **d** and **e** flg22-induced ROS production. Leaf discs from 28-day-old plants were treated with 200 nM flg22.
1013 Box plots show integration of ROS production for 40 min (upper right).

1014 **d** flg22-induced ROS production in *RBOHDpro::3FLAG-RBOHD/rbohD* #11-1 and *RBOHDpro::3FLAG-*
1015 *RBOHD^{S703A}/rbohD* #1-4. Values represent the mean \pm SEM of n = 24. Difference between lines was
1016 evaluated with One-way Anova (F value = 15.4533, DF = 1) with Tukey-Kramer HSD, *** p < 0.001.

1017 **e** flg22-induced ROS production in *RBOHDpro::3FLAG-RBOHD/rbohD* #11-1 and *RBOHDpro::3FLAG-*
1018 *RBOHD^{S862A}/rbohD* #11-5. Values represent the mean \pm SEM of n \geq 23. Difference between lines was
1019 evaluated with One-way Anova (F value = 5.1845, DF = 1) with Tukey-Kramer HSD, * p < 0.05.

1020

1021 **Fig. S8 Reduced ROS production in *crk2* is not due to lower expression of *BIK1*.**

1022 Box plot shows quantitative real-time RT-PCR (qPCR) analysis of *BIK1* transcripts in Col-0, *crk2* and *fls2*
1023 after treatment with flg22 (n = 3, biological replicates). 10-day-old plants were incubated in 1 μ M flg22
1024 solution and collected at indicated time (each time point contains 90 plants per genotype). Transcript levels
1025 were calculated by comparison with non-treated Col-0 (Time = 0). Different letters indicate significant
1026 difference at $p < 0.05$ [One-way Anova (F value = 220.6240, DF = 8) with Tukey-Kramer HSD].

1027

1028

1029 **Supplementary table legends**

1030 **Table S1. *In vitro* phosphorylation sites of 6His-MBP-RBOHDcyto by 6His-GST-CRK2cyto**

1031 The 6His-MBP-RBOHD cytosolic regions were incubated with 6His-GST-CRK2cyto. The 6His-MBP-
1032 RBOHDcyto bands were excised from a SDS polyacrylamide gel and subsequently digested by trypsin or Lys-C.
1033 The peptides were analyzed by LC-MS/MS. Phosphorylated peptides are designated as pS.

1034

1035 **Table S2. Progeny of *CRK2/crk2 BIK1/bik1* parent and *CRK2/crk2 bik1/bik1* parent**

1036 The genotypes of F2 and F3 progenies were determined by PCR. Observed, the number of individuals observed;
1037 Expected, the expected number based on Mendelian inheritance. Chi-square test was used to determine the
1038 probability (P) of which the deviation of the observed value from the expected value was due to chance.

1039

1040 **Table S3. Primer sequences**

1041

1042

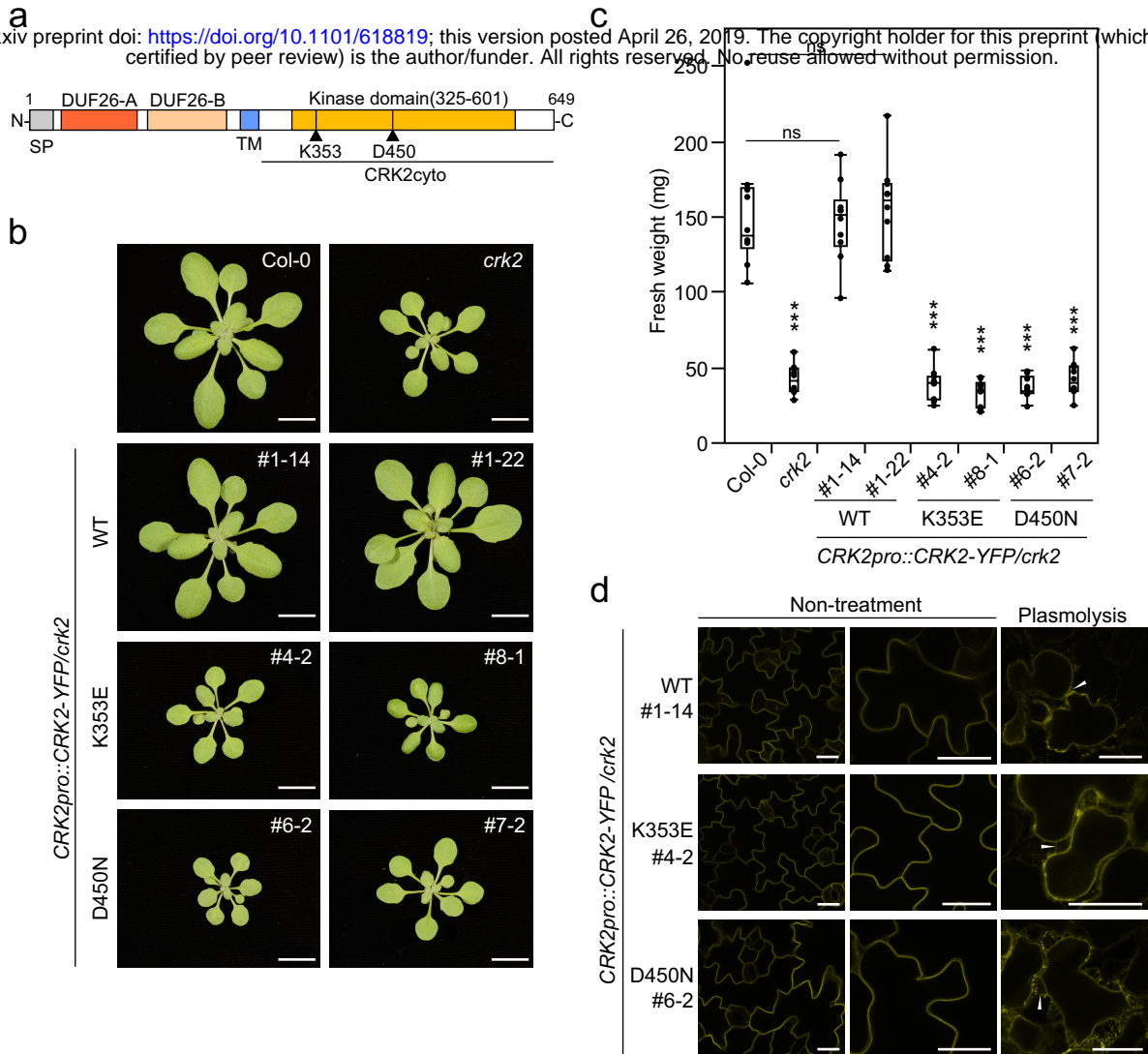


Fig. 1 CRK2 kinase activity is required for plant growth.

a Schematic representation of CRK2 structure. SP: signal peptide (AAs 1-29), DUF26-A (AAs 39-132), DUF26-B (AAs 146-243), TM: transmembrane domain (AAs 261-283), and kinase domain (AAs 325-601). **b** Representative pictures of 21-day-old plants of Col-0, *crk2*, *CRK2pro::CRK2-YFP/crk2*, *CRK2pro::CRK2^{K353E}-YFP/crk2* and *CRK2pro::CRK2^{D450N}-YFP/crk2* plants. Bar = 1 cm. **c** Box plot shows the fresh weight of 21-day-old plants (n = 10). Differences between Col-0 and transgenic lines were evaluated with One-way Anova with Tukey-Kramer HSD, *** p<0.001, ns, not statistically significant (Oneway Anova, F value = 71.5559, DF = 7). The experiment was repeated three times with similar results. **d** Subcellular localization of CRK2-YFP, CRK2^{K353E}-YFP and CRK2^{D450N}-YFP in leaves of 7-day-old seedlings. Plasma membrane localization was confirmed using plasmolysis to visualize Hechtian strands (arrow heads). Plasmolysis was induced by the application of 0.8 M mannitol. Scale bar = 25 μ m.

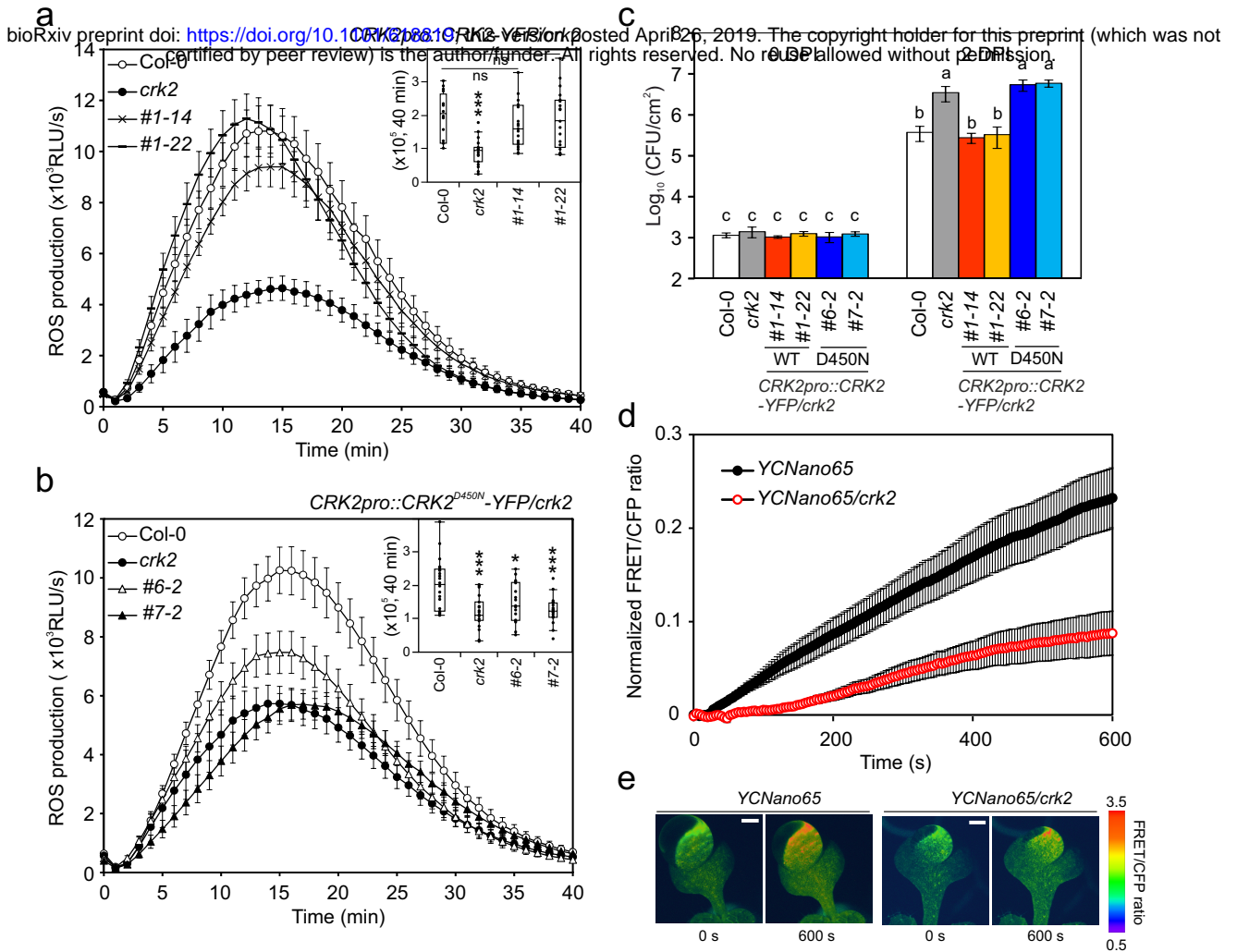


Fig. 2 CRK2 regulates flg22-triggered immunity and resistance to a virulent bacterial pathogen.

a and **b** flg22-induced ROS production in Col-0, *crk2* and *CRK2pro::CRK2*-YFP/*crk2* or *CRK2pro::CRK2^{D450N}*-YFP/*crk2*. Leaf discs from 28-day-old plants were treated with 200 nM flg22 and ROS production was measured. Box plot shows cumulative ROS production over 40 min (upper right). **a** Values represent mean \pm SEM of $n \geq 16$. Differences compared with Col-0 were evaluated with One-way Anova (F value = 9.2282, DF = 3) with Tukey-Kramer HSD, *** $p < 0.001$, ns, not statistically significant. **b** Values represent the mean \pm SEM of $n \geq 19$. Differences compared with Col-0 were evaluated with One-way Anova (F value = 8.8777, DF = 3) with Tukey-Kramer HSD, * $p < 0.05$, *** $p < 0.001$. **c** Quantitative analysis of bacterial growth in Col-0, *crk2* and *CRK2pro::CRK2*-YFP/*crk2* or *CRK2pro::CRK2^{D450N}*-YFP/*crk2* following syringe infiltration with *Pto* DC3000 (1×10^5 CFU/mL). Values represent mean \pm SD of $n = 3$ (0 DPI) or $n = 6$ (2 DPI). Letters indicate significant differences at $p < 0.05$ [One-way Anova (F value = 566.5661, DF = 11) with Tukey-Kramer HSD]. **d** Quantitative analysis of cytosolic Ca²⁺ changes in response to 10 μ M flg22 in 7-day-old YCNano65 or YCNano65/*crk2* seedlings. Values represent the mean \pm SEM of $n = 9$ (YCNano65) or $n = 15$ (YCNano65/*crk2*). **e** Representative frame images of cytosolic Ca²⁺ change in wild type and *crk2* plants. Bar = 0.5 mm. **a - e** The experiment was repeated three times with similar results.

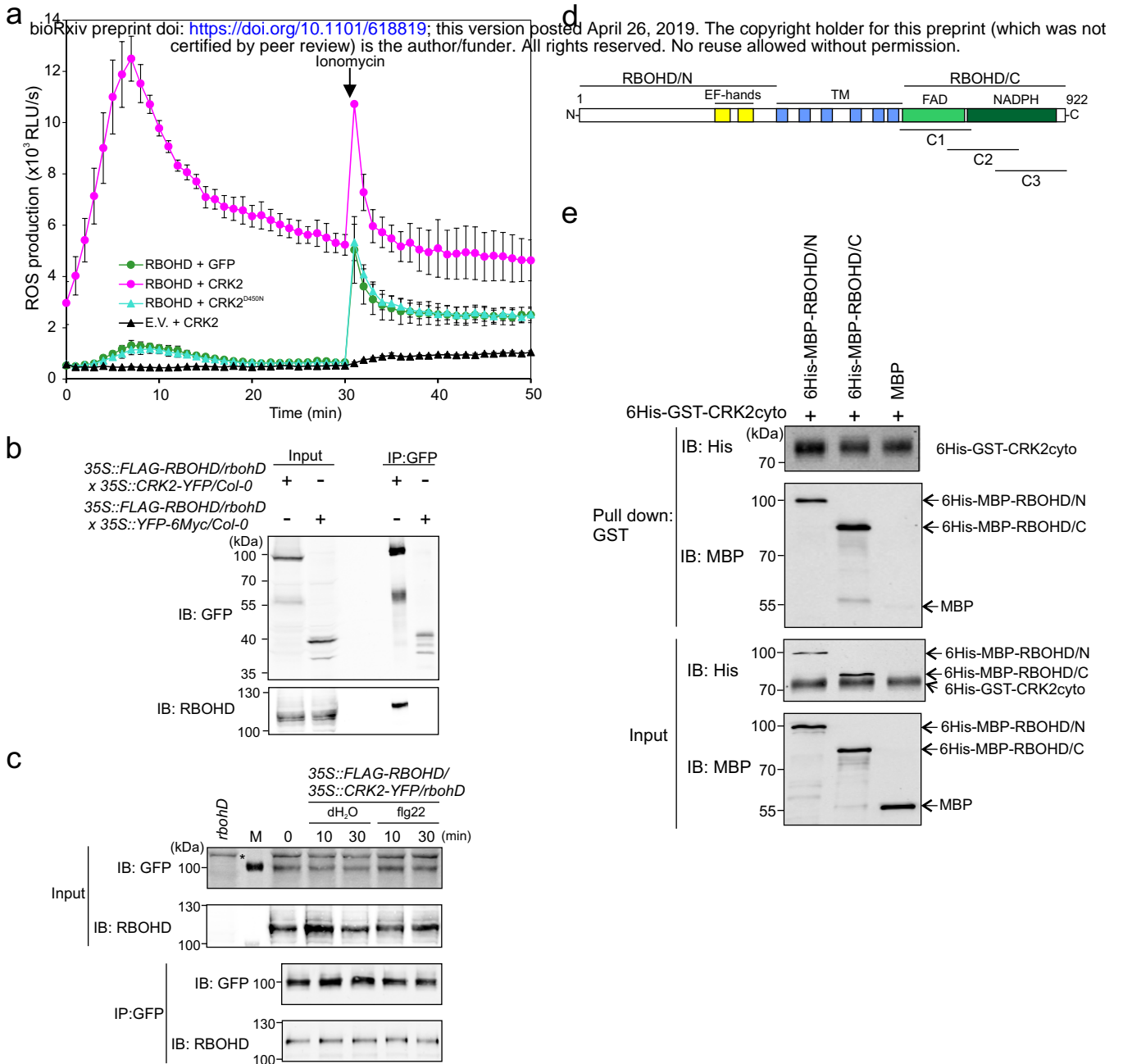


Fig. 3 CRK2 interacts with RBOHD.

a ROS production of RBOHD-expressing HEK293T cells. 3FLAG-RBOHD was transiently co-expressed with either 3Myc-GFP or CRK2 (WT or D450N)-3Myc. After 30 min $1 \mu\text{M}$ ionomycin was added to the medium. Values represent mean \pm SEM of $n = 3$. E.V. = empty vector. The experiment was repeated three times with similar results. **b** and **c** Co-IP analysis of interaction between RBOHD and CRK2. CRK2-YFP was immuno-precipitated using anti-GFP beads followed by immunoblotting with anti-RBOHD and anti-GFP antibodies. FLAG-RBOHD: 105 kDa, CRK2-YFP: 99.9 kDa and YFP-6Myc: 36.7 kDa. **b** 35S::FLAG-RBOHD/*rbohD* x 35S::CRK2-YFP/*Col-0* (F1) and 35S::FLAG-RBOHD/*rbohD* x 35S::YFP-6Myc/*Col-0* (F1) plants. The experiment was repeated three times with similar results. **c** 35S::FLAG-RBOHD/35S::CRK2-YFP/*rbohD* plants with $1 \mu\text{M}$ flag22 treatment. M: Protein molecular marker, *: unspecific signal. Total protein from *rbohD* was used for immunoblot of input as a negative control. **d** Schematic representation of RBOHD structure. EF-hands (AAs 257-329), TM: transmembrane domains (AAs 374 - 605), FAD: FAD-binding domain (AAs 613-730), NADPH: NADPH-binding domain (AAs 736-904), RBOHD/N: RBOHD N-terminal region (AAs 1-376), RBOHD/C: RBOHD C-terminal region (AAs 606-922); C1: RBOHD/C1 (AAs 606-741), C2: RBOHD/C2 (AAs 696-831), C3: RBOHD/C3 (AAs 787-922). **e** In vitro pull-down analysis of direct interaction between RBOHD and CRK2. MBP, 6His-MBP-RBOHD/N and 6His-MBP-RBOHD/C were incubated with 6His-GST-CRK2cyto and pull down with GST followed by immunoblotting with anti-6His and anti-MBP antibodies. 6His-GST-CRK2cyto: 68.5 kDa, 6His-MBP-RBOHD/N: 84.7 kDa, 6His-MBP-RBOHD/C: 78.4 kDa, MBP: 50.8 kDa. The experiment was repeated two times with similar results.

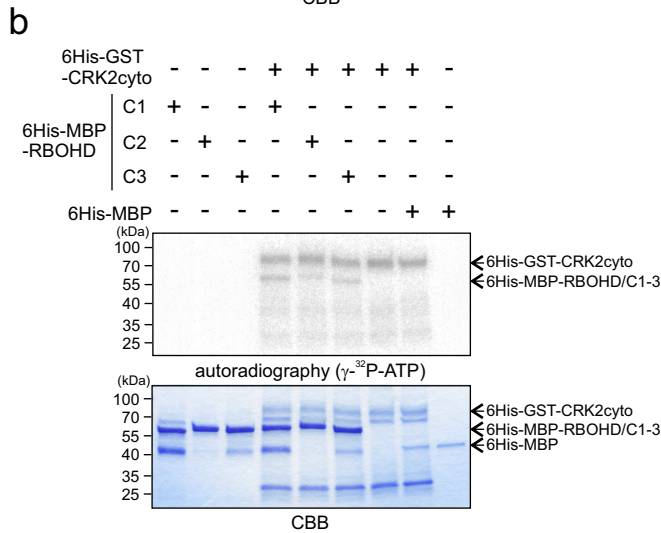
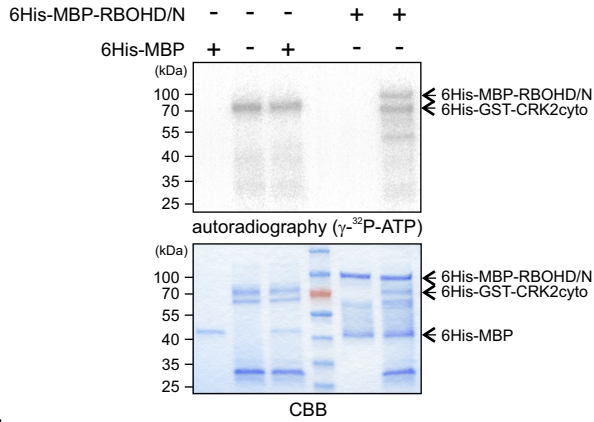


Fig. 4 CRK2 phosphorylates the cytosolic regions of RBOHD *in vitro*.

a and **b** Autophosphorylation and transphosphorylation were visualized with [γ - 32 P] ATP and autoradiography (upper panel). Input proteins were stained with coomassie brilliant blue (CBB) (lower panel). Experiments were repeated three times with similar results. 6His-GST-CRK2cyto: 68.5 kDa, 6His-MBP-RBOHD/N: 84.7 kDa, 6His-MBP-RBOHD/C1:57.9 kDa, /C2:57.8 kDa, /C3:58.4 kDa, 6His-MBP: 44.3 kDa. **a** *In vitro* transphosphorylation of 6His-MBP-RBOHD N-terminus by 6His-GST-CRK2cyto. 6His-MBP-RBOHD/N or 6His-MBP was incubated with 6His-GST-CRK2cyto in kinase buffer. **b** *In vitro* transphosphorylation of 6His-MBP-RBOHD C-terminus by 6His-GST-CRK2cyto. 6His-MBP-RBOHD/C1, /C2, /C3 or 6His-MBP was incubated with 6His-GST-CRK2cyto in kinase buffer.

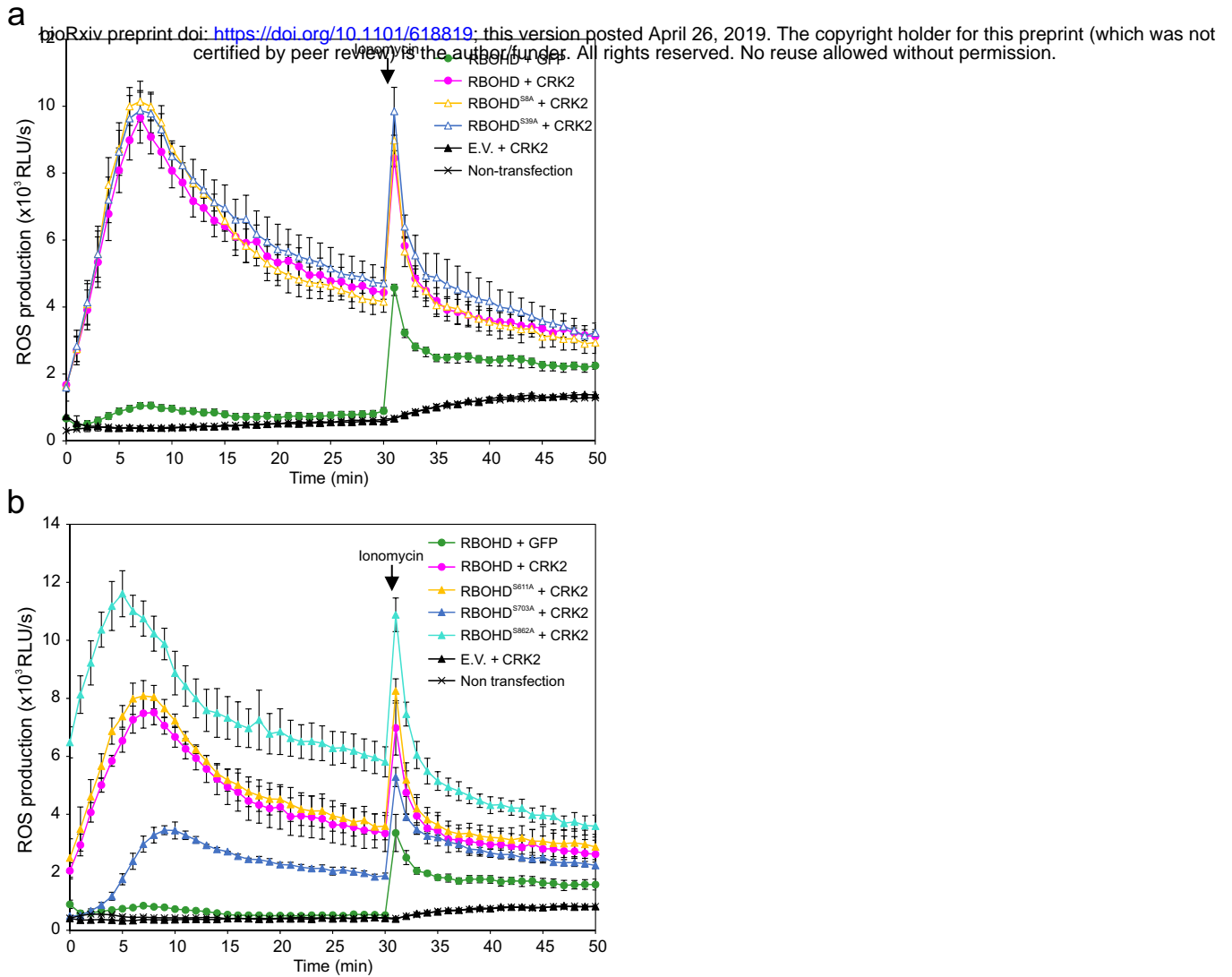


Fig. 5 CRK2 modulates the ROS-production activity of RBOHD via phosphorylation of the C-terminus in HEK293T cells.

a Effect of mutations of CRK2-dependent *in vitro* phosphorylation sites in the N-terminal cytosolic region of RBOHD. 3FLAG-RBOHD (WT, S8A or S39A) was transiently co-expressed with either 3Myc-GFP or CRK2-3Myc in HEK293T cells. After 30 min 1 μ M ionomycin was added to the medium to promote Ca^{2+} influx. Values represent mean \pm SEM of $n = 3$. E.V. = empty vector. The experiment was repeated three times with similar results. **b** Effect of mutations in the CRK2-dependent *in vitro* phosphorylation sites in the C-terminal cytosolic region of RBOHD. 3FLAG-RBOHD (WT, S611A, S703A or S862A) were transiently co-expressed with either 3Myc-GFP or CRK2-3Myc in HEK293T cells. After 30 min 1 μ M ionomycin was added to the medium to promote Ca^{2+} influx. Values represent mean \pm SEM of $n = 3$. E.V. = empty vector. The experiment was repeated three times with similar results.

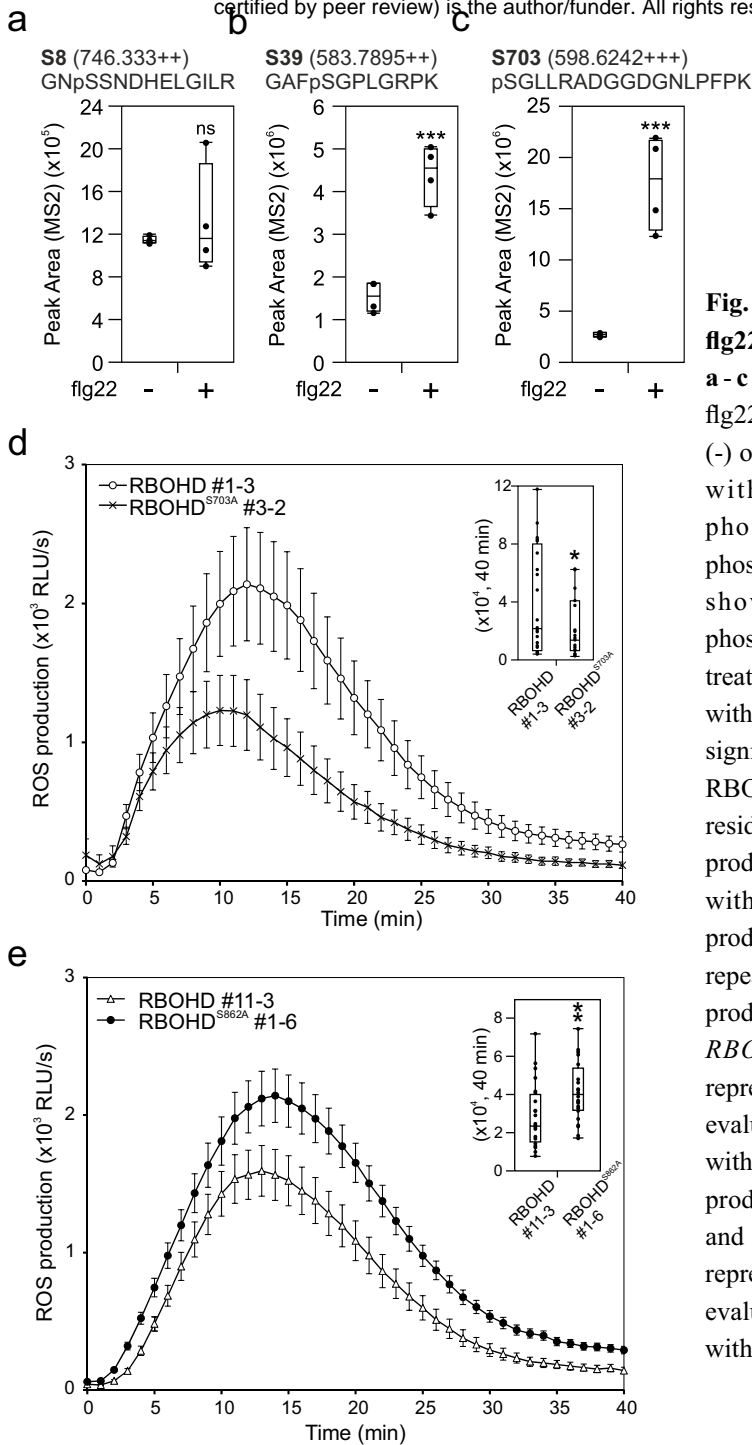


Fig. 6 RBOHD S703 and S862 are involved in regulation of flg22-induced ROS production.

a - c Quantification of RBOHD phosphorylation in Col-0 upon flg22 treatment. 12-day-old seedlings were treated with water (-) or 1 μ M flg22 (+) for 5 min. Total proteins were digested with trypsin (S8 and S39) or Lys-C (S703) and phosphopeptides were enriched, and then selected phosphopeptides were quantified by LC-MS/MS. Box plots show MS2 fragment peak ion areas of indicated phosphopeptides ($n = 4$). Differences between water- or flg22-treated samples were evaluated with One-way Anova (DF = 1) with Tukey-Kramer HSD, *** $p < 0.001$, ns, not statistically significant. **a** RBOHD S8 residue (F value = 0.4745). **b** RBOHD S39 residue (F value = 51.3297). **c** RBOHD S703 residue (F value = 41.0851). **d** and **e** flg22-induced ROS production. Leaf discs from 28-day-old plants were treated with 200 nM flg22. Box plot shows cumulative ROS production over 40 min (upper right). The experiment was repeated three times with similar results. **d** flg22-induced ROS production in *RBOHDpro::3FLAG-RBOHD/rbohD* #1-3 and *RBOHDpro::3FLAG-RBOHD^{S703A}/rbohD* #3-2. Values represent mean \pm SEM of $n \geq 23$. Difference between lines was evaluated with One-way Anova (F value = 4.4509, DF = 1) with Tukey-Kramer HSD, * $p < 0.05$. **e** flg22-induced ROS production in *RBOHDpro::3FLAG-RBOHD/rbohD* #11-3 and *RBOHDpro::3FLAG-RBOHD^{S862A}/rbohD* #1-6. Values represent mean \pm SEM of $n = 24$. Difference between lines was evaluated with One-way Anova (F value = 8.5305, DF = 1) with Tukey-Kramer HSD, ** $p < 0.01$.

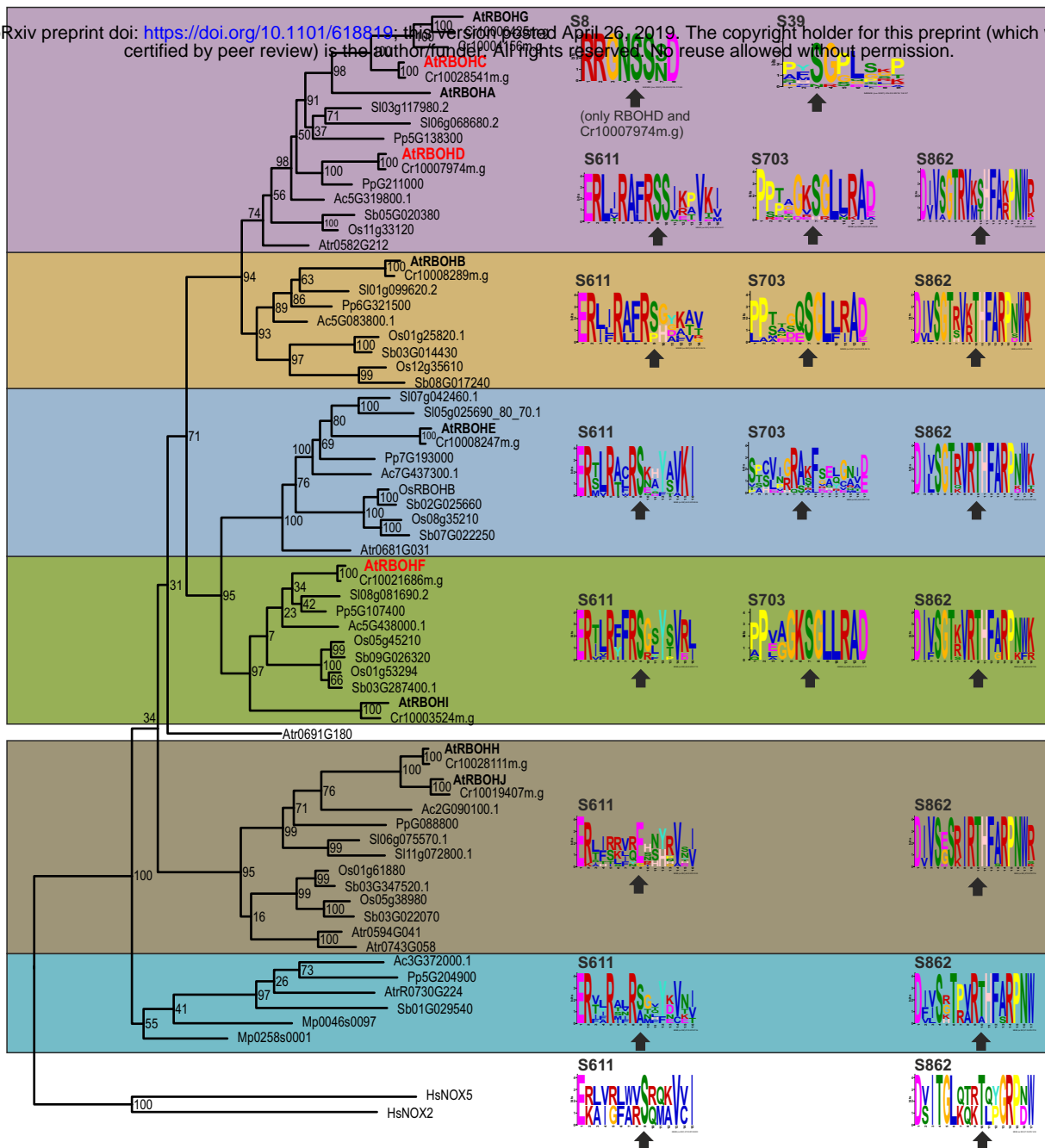


Fig. 7 Phosphorylation sites in the C-terminal region are conserved in plants and animals.

Phylogenetic tree showing that plant RBOHs form a single clade which is parallel to the NADPH oxidases NOX2 and NOX5 β from *Homo sapiens*. The sequence context of the phospho-site S8 in RBOHD is only conserved RBOHD from *Arabidopsis thaliana* and *Capsella rubella*. The tree was constructed using FASTTREE from a PAGAN alignment in WASABI, 100 bootstraps were calculated with RAxML. The full sequence alignment can be found in Wasabi at <http://was.bi?id=JauZ6q>. Plant species included were: *Arabidopsis thaliana* (At), *Capsella rubella* (Cr), *Prunus persica* (Pp), *Solanum lycopersicum* (Sl), *Aquilegia coerulea* (Ac), *Oryza sativa* (Os), *Sorghum bicolor* (Sb), *Amborella trichopoda* (Atr), and *Marchantia polymorpha* (Mp). Numbers of phospho-sites in the meme figures represent the position of the amino acid in RBOHD from *Arabidopsis thaliana*. Arrows indicate the position of the phospho-site (S or T) or corresponding amino acid.

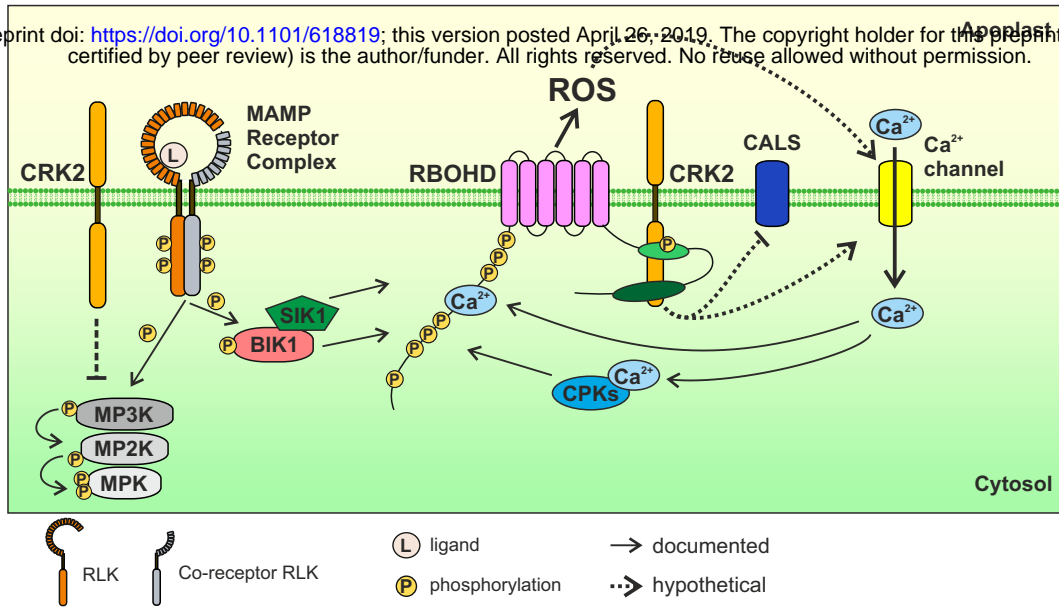


Fig. 8 Schematic model for MAMP-triggered RBOHD activation.

MAMPs are recognized by MAMP receptor complexes. RBOHD N-terminus is phosphorylated by BIK1 and SIK1 and apoplastic ROS production is induced. Apoplastic ROS production by RBOHD leads to Ca²⁺ influx into the cytosol. Ca²⁺-binding to RBOHD N-terminus and to CPKs leads to Ca²⁺-dependent activation of RBOHD. We found that CRK2 also contributes to the activation of RBOHD *via* phosphorylation of its C-terminus at S703. CRK2 can also mediate inhibition of MAPK activation and callose deposition *via* CALS after MAMP perception. MPK, mitogen-activated protein kinase; MP2K, MPKK; MP3K, MPKKK.